Biomass Conversion and Biorefinery (2025) 15:15361–15384
https://doi.org/10.1007/s13399-024-06229-2

ORIGINAL ARTICLE

Biochemical and cytological studies of *Typha domingensis* used for bioethanol production

Rehab M. Hafez[1] · Tahany M. A. Abdel-Rahman[1] · M. Mokhtar Yahia[2] · Khadiga I. M. El-Gabry[3] · Yosra M. M. Abdel Wahab[1]

Received: 21 July 2024 / Revised: 15 September 2024 / Accepted: 1 October 2024 / Published online: 30 October 2024

Abstract
Typha domingensis (cattails) is an emergent invasive aquatic macrophyte; it belongs to Typhaceae family inhabiting multiple Egyptian water bodies like rivers, lakes, and wetlands. Due to the scarcity of food, the depletion of fossil fuels, population growth, and increased industrial development, sustainable renewable bioenergy production has gained a lot of attention lately. Typha is an excellent lignocellulosic biomass for biofuel production because it does not compete with food but rather endangers aquatic life and prevents water from flowing through drainage channels and canals, which rises evapotranspiration. Although it is beneficial in phytoremediation, its removal is a necessity due to previous reasons. Chemical pretreatment has been widely used to degrade complex chains of lignocellulosic materials. Enzymatic hydrolysis is used to enhance fermentable sugars production from cellulose. Fermentation process has been conducted by yeast for centuries. *Saccharomyces cerevisiae* tolerance to ethanol can be increased by mutation; it is induced either chemically, physically, or biologically. Geneticists frequently utilize gamma radiation, one of the physical mutagenesis mechanisms, to change the DNA of microorganisms. Scanning electron microscope (SEM) is concerned with examination and analysis of microstructure morphology and chemical composition. Changes in internal organelles of *Saccharomyces cerevisiae* after mutation has been tracked using transmission electron microscope (TEM) in order to distinguish between native and mutant yeast and to examine their ultrastructural changes.

Keywords *Typha domingensis* · Cattail · Pretreatments · Yeast · Enzyme · Biofuel · Mutation · SEM · TEM

1 Introduction

Energy consumption has increased steadily over the last century as the world population has grown and more countries became industrialized [1]. Bioenergy is viewed as a more environmentally friendly source of energy and is expected to solve the global warming problem, caused mainly by fossil fuels, through decreasing the greenhouse gas emission in the atmosphere and preventing further deforestation or otherwise the degradation of the local environment [2–5].

The first generation bioethanol was made from the sugars and vegetable oils found in arable crops, while the second one is based on lignocellulosic biomass from non-edible plants and agricultural residues or wastes, which are rich in complex carbohydrates like cellulose and lignocellulose [6]. Although crops yield high ethanol, we cannot compete with food sources and compromise on food security [7]. Therefore, more research has focused on using the second-generation bioethanol rather than the first one [8].

Aquatic weeds has been placed forward as a feasible alternative due to its abundance in nature, and the large quantities generated as waste in our local water bodies (*Eichhornia crassipes*, *Cyperus* sp., *Lemna* sp., *Phragmites* sp., *Typha* sp., etc.) do not compete with land resources used in arable food crop cultivation [9].

Typha spp. (Cattails) are herbaceous, monocotyledonous, perennial plants, belonging to the Typhaceae family

✉ Rehab M. Hafez
rehabhafez@sci.cu.edu.eg

[1] Department of Botany and Microbiology, Faculty of Science, Cairo University, Giza 12613, Egypt

[2] Central Laboratory for Environmental Quality Monitoring, National Water Research Center, Kanater El Khairia, Egypt

[3] Department of Agricultural Microbiology-Soils, Waters and Environmental Research Institute (SWERI) - Agricultural Research Center (ARC), Giza, Egypt

(order Poales) inhabiting fresh water/slightly mineralized wetlands. They have been proposed as promising biomass crop because they are non-food lignocellulosic feedstock with 47.6% cellulose and 21.9% lignin [10–12]. In addition, they are considered as an attractive raw material because of its availability in large quantities at low cost through the environment cleaning process [13]. Bioethanol production from agricultural products has been in practice for years which has created a direct competition between food and energy sector. For lignocellulosic material, they need to be converted to simple sugars through hydrolysis process before fermentation [14]. Hydrolysis process can be carried out in two steps chemical hydrolysis (acidic and/or alkaline) or enzymatic hydrolysis (from plant or microbes) [15]. *Saccharomyces cerevisiae* has been used through thousands of years, without strong competitors, for its ability to ferment glucose-rich hydrolysates for the production of bioethanol [16].

Mutagenesis, either by chemical or physical agents, is one of the preferred methods for strain improvement in microbes. Several investigations mentioned to use this technique to improve yeast for ethanol production [17].

The aim of this study was to evaluate the different pretreatments employed on cattail plant material (chemically and cytologically) and to select the best technique for the production of reasonable amount of bioethanol using native and mutant yeast strains.

2 Materials and methods

2.1 Plant material

Typha domingensis (southern cattail) was kindly provided from El-Manzala lake project, National Water Research Center, Ministry of Water Resources and Irrigation, Egypt (Fig. 1).

2.2 Yeast strain

The yeast strain *Saccharomyces cerevisiae* was obtained from Egyptian company of Sugar and Integrated Industries, Egypt.

2.3 Yeast growth and maintenance

The yeast strain was streaked and cultured for 2 days in dark at 28 °C on sterile Petri-dishes containing sterilized solidified yeast peptone dextrose agar medium (YPD). Each liter of YPD medium contains: 1% (w/v) yeast extract; 2% (w/v) peptone; 2% (w/v) D-glucose and solidified with 2% agar.

Fig. 1 *T. domingensis* (southern cattail)

2.4 Fungal species

Aspergillus versicolor was used to prepare the crude hydrolyzing enzyme. It was generously offered by Department of Microbiology, Soils, Water and Environment Research Institute (SWERI), Agriculture research center (ARC), Egypt, and it was prepared following the method of [18].

2.5 Water analyses

Water sample was collected from El-Manzala lake, from which cattail plants were collected; it was utilized in preparing growth medium. The water sample was subjected to chemical analyses (BOD, COD, NH3, and heavy metals) and microbiological analyses (total and fecal coliform) (Table 1).

Those analyses were performed in the Central Laboratories of Environmental Quality Monitoring of the National Water Research Center (NWRC) according to the standard method of [19].

2.6 Feedstock processing/preparation of the cattail powder

Whole, fresh cattail plants were collected, washed with tap water then with distilled water. The clean plants were cut into parts of 1 cm length and dried in oven at 60 °C until constant weight [20]. Dried plants were grinded with grinder mill to reduce the particle size to fine powder. The powders

Table 1 Estimated water physicochemical parameters analyzed from El-Manzala lake

Physicochemical parameters (mg/L)	
BOD	22.29 ± 2.19
COD	62.14 ± 5.36
NH_3	1.23 ± 0.36
Trace metals (mg/L)	
Aluminum (Al)	0.134 ± 0.05
Antimony (Sb)	< 0.009 ± 0.00
Arsenic (As)	< 0.002 ± 0.00
Barium (Ba)	0.066 ± 0.00
Cadmium (Cd)	< 0.002 ± 0.00
Chromium (Cr)	< 0.002 ± 0.00
Cobalt (Co)	< 0.003 ± 0.00
Copper (Cu)	0.023 ± 0.01
Iron (Fe)	0.162 ± 0.04
Lead (Pb)	< 0.007 ± 0.00
Manganese (Mn)	0.081 ± 0.03
Nickel (Ni)	0.028 ± 0.00
Selenium (Se)	< 0.007 ± 0.00
Tin (Sn)	< 0.006 ± 0.00
Vanadium (V)	< 0.001 ± 0.00
Zinc (Zn)	< 0.005 ± 0.00
Microbiological parameters (CFU/100 ml)	
Total coliform	15×10^3
Fecal coliform	12×10^3

Each value represents the mean of seven replicates ± SD.

were stored in air tight-capped containers at room temperature until further usage.

2.7 Optimization of the pretreatment process

Acid/alkaline pretreatments were prepared according to the method of [1]. Pretreatment was carried out in tight-capped bottles (100 ml) by mixing 3 g of dried cattail powder with different acids and alkali concentrations, separately.

2.7.1 Acid pretreatment

H_2SO_4, HCL, and CH_3COOH were tested as acid pretreatments. Three-gram dried cattail powder were mixed with 1%, 2%, 3%, and 4% (v/v) concentrations of each acid in tight-capped bottles (100 ml) according to [1]. Each treatment was prepared in triplicates. The mixtures were left overnight at room temperature. Each mixture was autoclaved at 121 °C, 15 Ibs for 15 min and cooled down to room temperature. The hydrolysate was filtered using Whatman filter paper (No. 1) to remove unhydrolyzed material. The filtered pretreated solid residues of the best acid pretreatment process were air dried and prepared for scanning microscopy (SEM) and FTIR. Each filtrate was collected and analyzed for reducing sugar content by dinitrosalicylic acid test (DNS) according to [21].

2.7.2 Alkaline pretreatment

Alkaline pretreatment was carried out by mixing 3 g of dried cattail powder with 1%, 2%, 3%, and 4% v/v concentrations of each alkali (NaOH/KOH/NaClO) in tight-capped bottles (100 ml) according to Awasthi et al. (2013). The mixtures were left overnight at room temperature. Each mixture was autoclaved at 121 °C, 15 Ibs for 15 min and cooled down to room temperature. Each hydrolysate was filtered using Whatman filter paper (No. 1) to remove unhydrolyzed material. The solid unhydrolysate materials of the best alkaline pretreatment process was air dried and prepared for SEM and FTIR. Each filtrate (triplicates) was grouped and analyzed for reducing sugar content by di nitro salicylic acid test [21].

The best hydrolyser (acid/alkaline concentrations) which gave max reducing sugar contents using DNS test was combined with enzyme pretreatment in the next experiment.

2.7.3 NaClO/enzyme pretreatment

Ten grams of powder cattail was suspended in 200 ml of 4% of the best hydrolyser at pH 11.5 (0.3 ml NaClO/g substrate) in a 500 ml-conical flask (triplicates). The suspension was shaking overnight (100 rpm) at room temperature. The pretreated solutions were filtered through double layered muslin cloth, neutralized (pH 6.5–7.0) using 1N HCl solution, and then thoroughly washed with distilled water. The filtered pretreated solid unhydrolysate residues were air dried and prepared for SEM and FTIR. The filtrates (triplicates) were mixed and analyzed for reducing sugar content by di nitro salicylic acid test. Enzymatic pretreatment experiment was carried out at 50 °C using 2.5% (w/v) of each pretreatment biomass in 25-ml conical flasks with a total volume of 10 ml (0.05 M citrate buffer, pH 4.8). The flasks were stirred at 150 rpm in a shaking incubator at 50 °C for 48 h and then centrifuged at 4000 rpm for 15 min, and the supernatant was analyzed for total reducing sugars [22].

2.8 Fermentation medium (FM)

The enriched cultures from fungal strain were maintained to 0.5% dry biomass (w/v) and were used for inoculating (5%, v/v corresponding to 0.1 g dry biomass/20 ml) the fermentation medium volume of 150 ml medium in 200-ml firmly closed bottles to maintain minimized aeration conditions for fermentation process [23]. The FM structure was based on modified Mandels medium [24] with further modifications as follows: 100 g/L glucose as the sole carbon source and 47 g/L $(NH_4)_2SO_4$ as the sole nitrogen source, 0.1% yeast

extract and initial pH was adjusted at 5. Inoculated fermentation bottles allocated in a complete randomized design with three replicates were statically incubated at 30 °C for 24 h, and samples were collected at 2-day intervals for further studies.

2.9 Determination of reducing sugar using DNS method

The total reducing sugar was determined using di nitro salicylic acid test (DNS) reagent according to the method of [21].

Three milliliters of DNS reagent was added to 3 ml of each hydrolyzed samples in separated test tubes. The mixtures were heated for 5–15 min in a boiling water bath and then cooled under running tap water. Further, 1 ml of 40% potassium tartrate solution was added to stabilize the developed color. The color intensities were measured with spectrophotometer at 575 nm.

2.10 Ethanol determination using dichromate-titrimetric method

The applied method was performed according to the descriptive method of [25].

One milliliter sample in 20 mL $K_2 Cr_2 O_7$ solution was added to 50-mL volumetric flask. Collect ca 20 mL distillate to give ca 40 mL. Rinse outside of condenser outlet with water, and let rinse drain into flask. Stopper flask and immerse above liquid level in 37 ± 1 °C water bath. Remove flask after 10 min and immediately dilute contents to volume with 37 °C water, mix, and read ethanol concentration (% v/v at 15.56 °C) in the standardized spectrophotometer. If spectrophotometer does not have concentration mode, calculate ethanol concentration as follows:

$$\%EtOH = (As/Astd) \times 18.51$$

$$\text{Ethanol production yield} = \frac{\text{Ethanol (g/L)} \times 100}{\text{Initial Glucose (g/L)}}$$

$$\text{Ethanol production efficiency} = \frac{\text{Ethanol (g/L)} \times 100}{\text{Consumed Glucose (g/L)} \times 0.52}$$

2.11 FTIR method of analysis

FTIR analyses were conducted in CURP, Faculty of Agriculture, Cairo University. A part of each dry ground samples (control and treatments) was mixed with an excess of KBr (about 0.1–2% sample/KBr amount) to form a uniform consistency. The samples were analyzed using NICOLET 380 FT-IR, Thermo Scientific.

2.12 Transmission *electron* microscope

The method used for semi-thin sections was that described by [26], while that for ultra-thin sections was as reported by [27]. The *S. cerevisiae* samples (native and radiated) were fixed in glutaraldehyde and osmium tetroxide, dehydrated in alcohol, and embedded in an epoxy resin. Semi-thin sections were cut at thickness 500–1000 µm with a Leica ultracut UCT ultramicrotome, then stained with toluidine blue (1X), and examined by camera Leica ICC50 HD.

Ultra-thin sections of 75–90 µm thickness were stained with uranyl acetate and lead citrate [28] and then examined by transmission electron microscope JEOL (JEM-1400 TEM) at candidate magnification. Images were captured by CCD camera model AMT, optronics camera with 1632 × 1632 pixel formate as side mount configuration. This camera uses a 1394 fire wire board for acquisition.

2.13 Scanning *electron* microscope

The method used to prepare the samples for scanning electron microscopy was that described by [29].

Each tissue samples (each best treatments and control) were soaked in 3% glutaraldehyde for 1 h and washed three times with buffer. Then, the samples were passed through gradual series of ethyl alcohol (10–100%) each for 10 min before drying using critical point dryer. Each sample was concentrated to pallet affixed to stubs using double-sided sticky tape, and sputter coated with gold–palladium microscopy was performed with a JEOL GM 5200 microscope**.**

2.14 Gamma irradiation

S. cerevisiae sample was grown on 10 ml YPD medium overnight at 37 °C [OD_{680} = 0.54], then they were irradiated with 100, 300, 500, 1000 and 1500 Gy of ^{60}Co γ rays at a dose rate of 1.296 KGy/h for 5 min. The irradiation was carried out at National Center for Radiation Research and technology (NCRRT). The irradiated samples were separately inoculated in 10 ml YPD medium and incubated under the previously used conditions. The growth of the tolerant strain was monitored by optical density (OD_{680}) [30].

2.15 Growth curve

The growths of both native and irradiated yeasts were monitored by measuring ethanol yield at optical density of 680 nm at 12-, 24-h intervals. The best selected strains were also tested for ethanol yield measured at 12, 24, 36, and 48 h.

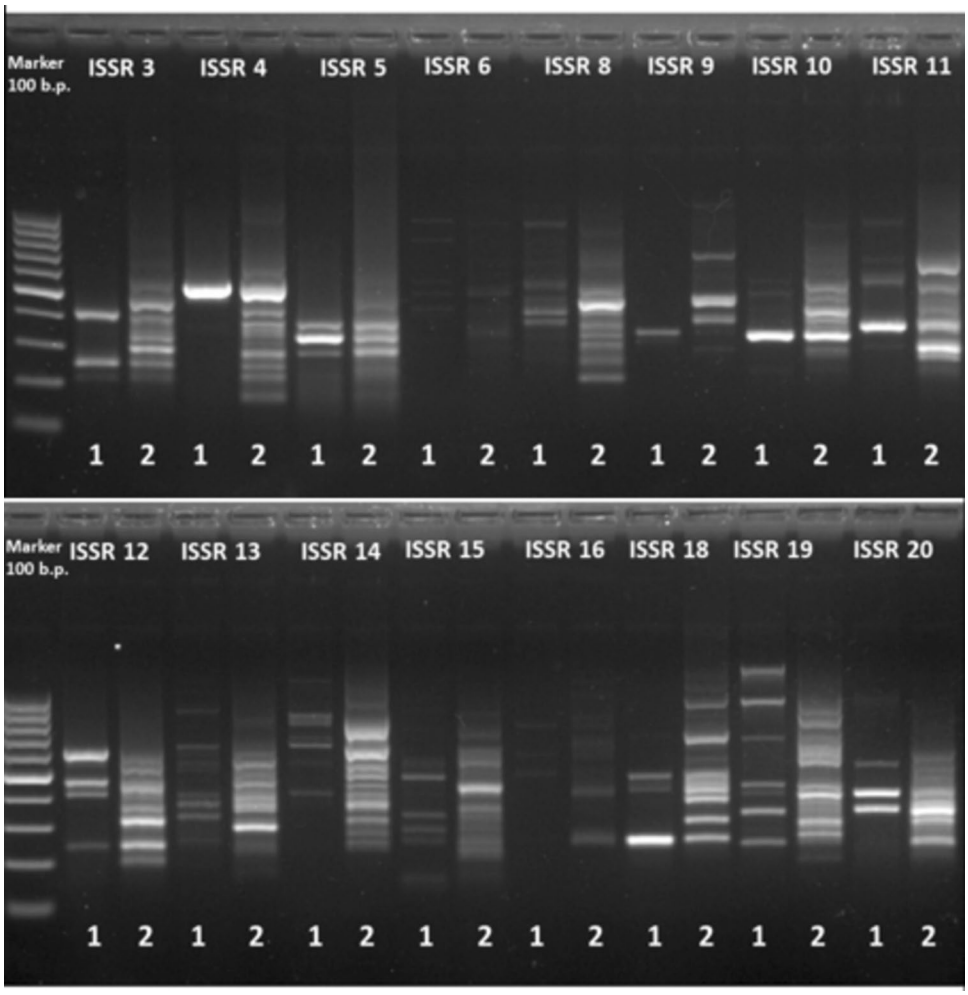

Fig. 2 ISSR banding patterns of native (1) and (2) mutant yeast using 16 primers

Table 2 Reducing sugars values after chemical pretreatment of cattail with different acids and alkalis

Conc (%)	Sulfuric acid (H_2SO_4)	Hydrochloric acid (HCl)	Acetic acid (CH_3COOH)	Potassium hydroxide (KOH)	Sodium hydroxide (NaOH)	Sodium hypochlorite (NaCLO)
1	24.40^{c}	22.31^{ef}	16.80^{k}	21.60^{gh}	22.50^{de}	21.02^{hi}
2	20.70^{l}	23.00^{d}	12.60^{n}	21.63^{gh}	25.50^{b}	19.70^{j}
3	14.43^{m}	21.68^{fg}	14.23^{m}	21.63^{gh}	25.55^{b}	22.07^{efg}
4	12.30^{n}	21.41^{gh}	15.40^{l}	26.03^{ab}	12.70^{n}	26.52^{a}
LSD 0.05	**0.637**					

Values followed by dissimilar letters with column are significantly different ($p < 0.05$); each value represents the mean of triplicates ± SD.

2.16 Determination of ethanol tolerance of native and mutant yeast strains

Ethanol tolerance determination was carried out according to [31].

Native and mutant yeasts were inoculated in 100 ml of YPD medium containing 15% (v/v) ethanol to achieve an initial cell density of 1×10^7 cells/ml. Triplicates were prepared for radiated inoculum. The cultures were grown with shaking (100 rpm) at 30 °C for 48 h. Cell samples were taken and spread using serially diluted method on solidified YPD and finally counted after incubation.

2.17 Molecular identification of native and mutant *S. cerevisiae*

Molecular methods were performed according to [31].

2.18 Extraction of DNA

Genomic DNA was isolated from native and radiated yeast via cetyltrimethylammonium bromide (CTAB) protocol. The concentrations of extracted DNA were measured using a Qubit® 3.0 Fluorometer (Thermo Fisher Scientific Inc.). For subsequent molecular analyses, DNA concentrations were adjusted to 10 ng/µl in all samples.

2.19 PCR analysis for ISSR

PCR amplifications were performed using 16 ISSR primers (Table 3) which produce clear reproducible pattern. For each primer, 25 µL amplification reaction contained 5 µL buffer (5 ×), 1.5 µL of genomic DNA (30 ng), 2 µL of 25 mM of $MgCl_2$, 0.5 µL of 10 mM dNTPs, and 0.15 µL of Taq DNA polymerase. DNA amplifications were performed using thermal cycler programmed (Applied Biosystems 2720) as follows: initial denaturation at 94 °C for 5 min followed by 40 cycles, denaturation at 94 °C for 50 s, annealing at 45 °C for 1 min, extension at 72 °C for 1 min, with final extension at 72 °C for 7 min. PCR products were separated on 1.5% agarose gels, stained with ethidium bromide, and visualized on UV. The gel in Fig. 2 was photographed using Bio-Rad Gel Documentation System.

2.20 Gas chromatography–mass spectrometry analysis (GC–MS) after native and mutant yeast strains fermentations

The GC–MS system (Agilent Technologies) was equipped with gas chromatograph (7890B), mass spectrometer detector (5977A), and headspace sampler (7697A) at Central Laboratories Network, National Research Centre, Egypt. Headspace temperature program represents oven temperature 70 °C, loop temperature 75 °C, and transfer line temperature 80 °C with an equilibrium time 10 min. The GC was equipped with HP-5MS column (30 m × 0.25 mm internal diameter and 0.25 µm film thickness). Analyses were carried out using helium as the carrier gas at a flow rate of 1.0 ml/min at a split mode 50:1, injection volume of 1 µl, and the following temperature program: 45 °C for 10 min; rising at 10 °C /min to 150 °C then held for 1 min. The injector and detector temperatures were held at 210 °C and 200 °C, respectively. Mass spectra were obtained by electron ionization (EI) at 70 eV using a spectral range of m/z 30–200. Identification of different constituents was determined by comparing the spectrum fragmentation pattern with those stored in Wiley and NIST Mass Spectral Library data of National Research Centre.

2.21 Statistical analysis

All experiments and analytical determinations were replicated three times, and the presented data are the mean values. The obtained results were subjected to one-way ANOVA (type of analysis depend on the factors affected

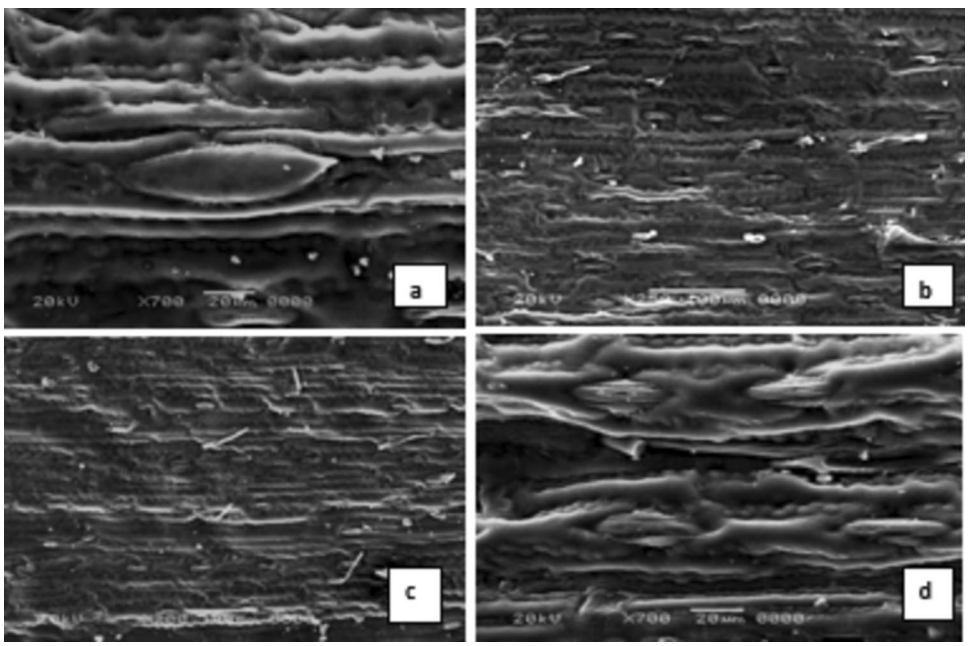

Fig. 3 SEM of fresh *T. domingensis* lower (**a**, **b**) and upper (**c**, **d**) leaf surface

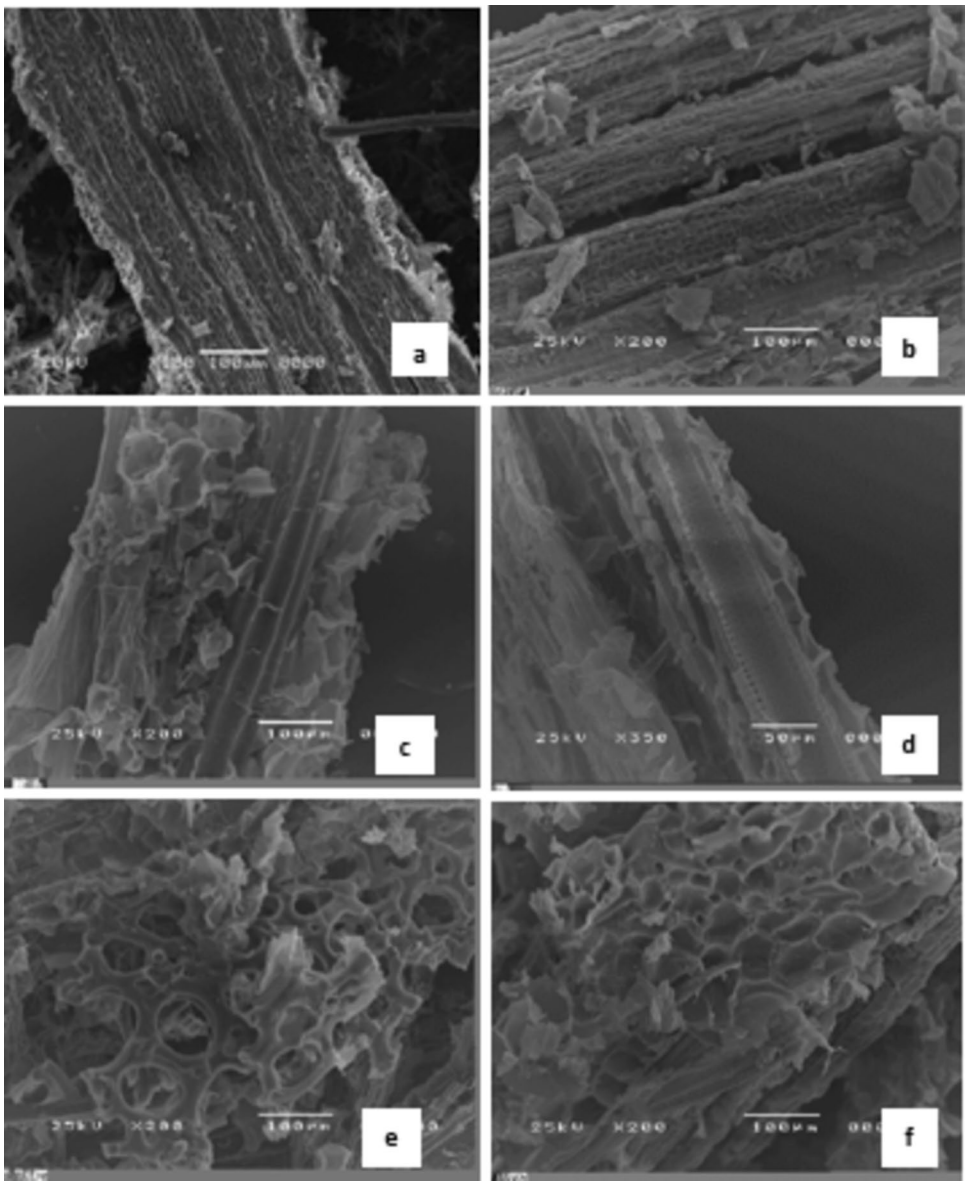

Fig. 4 SEM photograph of dried untreated (**a**) and pretreated (**b**–**f**) *T. domingensis* using **b** sulfuric acid, **c** acetic acid, **d** hydrochloric acid, **e** sodium hydroxide, and **f** potassium hydroxide

the experiment) to determine the significance between treatments using CoStat software [32].

3 Results and discussion

Microorganisms are of primary importance in the biofuel industry. The knowledge of the microbial metabolic processes, as well as their behavior and their technological characteristics, are required for any transformation process aiming to obtain biofuel/bioethanol [33].

Table 2 shows the amount of reducing sugars after chemical pretreatment of cattail with different acids (sulfuric acid, hydrochloric acid, and acetic acids) and alkalis (potassium hydroxide, sodium hydroxide, and sodium hypochlorite). Data revealed that 4% sodium hypochlorite produced the highest amount of reducing sugars (26.52 mg/ml) followed by 4% potassium hydroxide (26.03 mg/ml) and 3% sodium hypochlorite (25.55 mg/ml). However, acids have less effect on cattail tissues producing lower amounts of reducing sugars 16.80, 23.00, and 24.40 mg/ml for 1% acetic acid, 2% hydrochloric acid, and 1% sulfuric acid, respectively. This indicated that cattail may be susceptible to alkali pretreatments more than acids ones. It also revealed that sodium hypochlorite was the best among all the pretreatments used. Cattail is mostly composed of lignocellulose which should be pretreated to facilitate the biological fermentation process [34]. In terms of lignin-cellulosic material, untreated narrow leaves of cattail contain approximately 38.5–47.6% cellulose and 12.8–21.9% lignin [11, 34]. Hydrolysis is the process that must be used to transform the carbohydrate polymers in

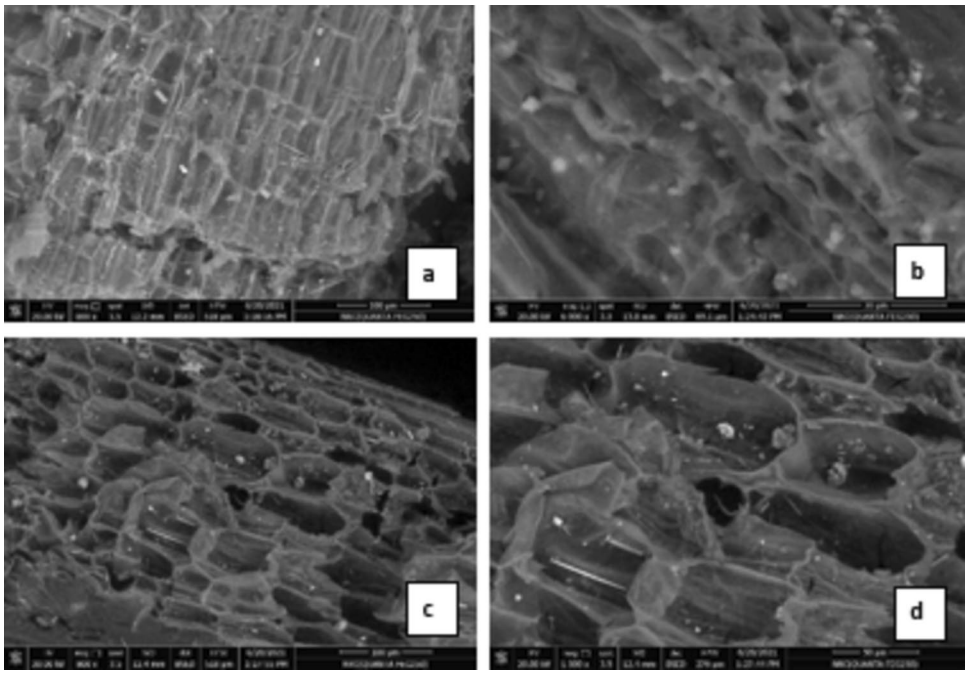

Fig. 5 SEM of dried cattail pretreated with sodium hypochlorite (**a**, **b**) and/or fungal enzyme (**c**, **d**)

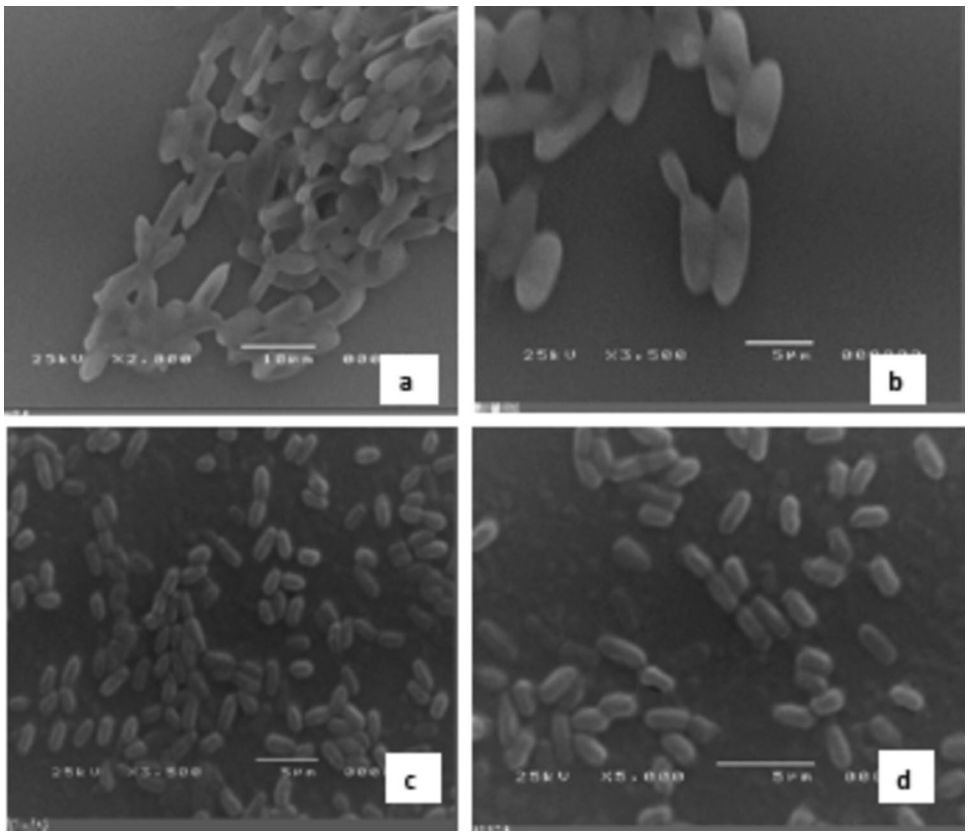

Fig. 6 SEM photograph of native (**a**, **b**) and mutant (**c**, **d**) irradiated *S. cerevisiae*

the lignocellulosic material into simple sugars in order to facilitate fermentation. There are various approaches that can be used to hydrolyze lignocelluloses. Chemical hydrolysis and enzymatic hydrolysis are the two categories into which the most widely used techniques fall [14]. Alkali and acid can be applied as the actual process of hydrolyzing lignocelluloses to sugars or as a pretreatment before enzymatic hydrolysis [1]. [35] found that by using

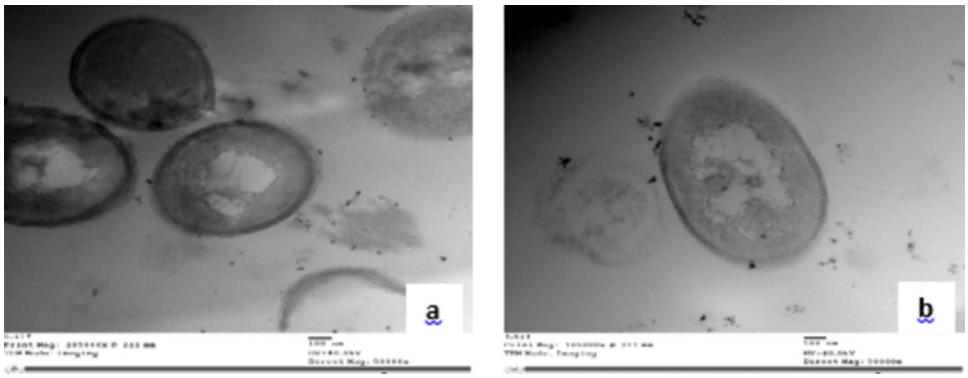

Fig. 7 TEM of native (**a**) and mutant (**b**) strain for *S. cerevisiae*

Table 3 Primer sequences

Primers	Sequences
ISSR 3	ACACACACACACACYT
ISSR 4	ACACACACACACACYG
ISSR 5	GTGTGTGTGTGTGTGTYG
ISSR 6	CGCGATAGATAGATAGATA
ISSR 8	AGACAGACAGACAGACGC
ISSR 9	GATAGATAGATAGATAGC
ISSR 10	GACAGACAGACAGACAAT
ISSR 11	ACACACACACACACACYA
ISSR 12	ACACACACACACACACYC
ISSR 13	AGAGAGAGAGAGAGAGYT
ISSR 14	CTCCTCCTCCTCCTCTT
ISSR 15	CTCTCTCTCTCTCTCTRG
ISSR 16	TCTCTCTCTCTCTCTCA
ISSR 18	HVHCACACACACACACAT
ISSR 19	HVHTCCTCCTCCTCCTCC
ISSR 20	HVHTGTGTGTGTGTGTGT

Similarity Matrix

	1	2
1	100%	
2	33%	100%

Fig. 8 Similarity matrix of native (1) and (2) mutant yeast

4% NaOH pretreatment on cattail leaves, about 60% of the lignin was dissolved in soluble form. A year later, [36] utilized dilute-sulfuric acid pretreatment on cattail leaves and found that it gave the highest total glucose yield for the pretreatment/hydrolysis stages (97.1% of the cellulose). Moreover, [34] reported that alkali pretreatment of cattail materials using 5% w/v NaOH increases the percentage of cellulose hydrolysis with the decrease in the percentage of both hemicellulose and lignin.

Pretreated *T. domingensis* with 4% sodium hypochlorite (best alkali) and crude enzyme of *A. versicolor* expressed the highest amounts of ethanol (3.53 g/L), fermentation yield (27.31), and percentage efficiency (34.29%). Fungal pretreatment is characterized by low energy consumption and minimal environmental impact, which has drawn attention to lignocellulose-degrading fungi. Numerous studies identified that lignocellulose-degrading fungi such as Ascomycetes and Basidiomycetes used both aerobic and anaerobic processes to break down cellulose: (1) extracellular enzymes and (2) the chelator-mediated Fenton system (CMF) [37, 38]. Anaerobic rumen fungi are a type of lignocellulose-degrading fungi that have cellulosomes containing both hemicellulolytic and cellulolytic enzymes [37]. In the lignolytic system, lignin peroxidase (LiP), manganese peroxidase (MnP), and laccase are the primary enzymes that break down lignin and release the phenyl rings [39–42].

Figure 3 illustrates the SEM photograph of Fresh *T. domingensis* lower and upper surfaces of the plant leaf. It indicated the adherence of fibers hemicellulose and lignin over the membrane surface. A study on SEM of the longitudinal section of *Typha* leaves and found that the leaf fibers are made up of ultimate fiber bundles of cellulose, which create the fibrous reinforcement. These bundles are connected by sticky and waxy substances, which form the matrix [43].

Figure 4a–f show SEM photograph of untreated and pretreated *T. domingensis* using Sulfuric acid, acetic acid, hydrochloric acid, sodium hydroxide, and potassium hydroxide. Figure 4a illustrates the compact feature of the plant cell wall (coherence of hemicellulose and lignin fibers shielding cellulose penetration). Sulfuric acid caused slight separation in hemicellulose and lignin fibers showing cellulose permeability (Fig. 4b). Acetic acid revealing its weak action over fibers although there is some pores appearing over membrane surface but was not strong enough to penetrate the cellulosic material (Fig. 4c). Hydrochloric acid expressed some fragmentation of the membrane fibers (hemicellulose and

Table 4 Different strains of *S. cerevisiae* (native and mutant) after ethanol tolerance test incubated for 12 h

Strains growth conditions		Ethanol amount (g/L)	Fermentation yield	Efficiency (%)
Gamma irradiation (Gy)	Concentration of ethanol tolerance (%)			
Control (-ve)	-	13.69	27.37	53.51^{bc}
	10%	12.00	24.00	46.92^{f}
	12%	13.49	26.99	52.76^{c}
	15%	12.00	24.00	46.92^{f}
100	-	13.85	27.70	54.15^{b}
	10%	13.74	27.47	53.71^{bc}
	12%	12.00	24.00	46.92^{f}
	15%	12.00	24.00	46.92^{f}
300	10%	14.55	29.11	56.90^{a}
500	10%	12.68	25.35	49.57^{e}
1500	12%	13.11	26.23	51.27^{d}
	15%	12.38	24.76	48.40^{e}
LSD (0.05)	**1.088**			

Values followed by dissimilar letters with column are significantly different ($p < 0.05$); each value represents the mean of triplicates ± SD.

Table 5 Different strains of *S. cerevisiae* (native and mutant) after ethanol tolerance test incubated for 24 h

Strains growth conditions		Ethanol (g/l)	Fermentation yield	Efficiency (%)
Gamma irradiation (Gy)	Concentration of ethanol tolerance (%)			
Control	-ve	17.26^{d}	34.54	67.53
	10%	16.85^{d}	33.71	65.90
	12%	9.82^{f}	19.65	38.42
	15%	19.15^{bc}	38.20	74.67
100	–-	19.26^{b}	38.54	75.35
	10%	14.13^{b}	28.26	55.26
	12%	19.10^{c}	36.62	71.59
	15%	18.31^{d}	34.95	68.33
300	10%	22.26^{a}	44.53	87.06
500	10%	17.47^{d}	34.90	68.24
1500	12%	19.18^{e}	38.37	75.01
	15%	8.93^{g}	17.87	34.94
LSD (0.05)	**1.3363**			

Values followed by dissimilar letters with column are significantly different ($p < 0.05$); each value represents the mean of triplicates ± SD.

lignin) showing more permeability of cellulose (Fig. 4d). Meanwhile, sodium hydroxide revealed high porosity in membrane fibers increasing its porosity (Fig. 4e). Potassium hydroxide action mimicking sodium hydroxide and made the membrane more porous and cellulose constituent became more exposed (Fig. 4f). The SEM photographs of dried *T. domingensis* pretreated with sodium hypochlorite revealed marked fiber disintegration with very high porosity of the membrane exposing large amount of cellulosic material (Fig. 5a, b). Comparing the impact of both pretreatments (acid and alkali) on the fine structure of cattail leaves tissues, it appeared that alkali produced high porosity than acid ones and the tissues under the acids pretreatment still have compact fibers but in shorter length. This may confirm the efficiency of alkali pretreatments toward removing the cementing materials in the lignocellulose tissues of cattail leaves. Pretreatment action is to breakdown the external fibers of lignin and hemicelluloses, reduce cellulose crystallinity, and increase the cellulose's surface and the porosity between the fibers of the tissues. The cellulose will be more soluble for enzymes to hydrolyzate and releasing glucose during the enzymatic hydrolysis of holocellulose to the solid residue [44–47]. In addition, [48] reported that dissociation of lignin from sugar molecules (cellulose and hemicellulose) through saponification of intermolecular ester bonds is one of the main processes that occur during the alkaline pretreatment process. More pentose sugar is preserved by alkaline pretreatment than by other pretreatment methods, increasing the amount of sugar production.

However, SEM photographs of dried cattail pretreated with sodium hypochlorite and fungal enzyme indicated prominent porosity along membrane fibers, in which most lignin and hemicellulose fibers fragmented and enhanced the

Table 6 Fermentation of the three best selected strains and control (-ve) at different time intervals (12, 24, 36, and 48 h)

Strains growth conditions		Hours											
		12			24			36			48		
Gamma irradiation (Gy)	Concentration of ethanol tolerance (%)	F.Y	Ethanol amount (g/L)	Efficiency (%)	F.Y	Ethanol amount (g/L)	Efficiency (%)	F.Y	Ethanol amount (g/L)	Efficiency (%)	F.Y	Ethanol amount (g/L)	Efficiency (%)
Control (-ve)		28.43	14.21	55.58^{g}	30.65	15.32	59.91^{f}	19.17	9.59	37.48^{k}	24.76	12.38	48.40^{j}
100 Gy	-	40.48	20.24	79.15^{b}	36.28	15.14	70.92^{d}	27.12	13.56	53.03^{h}	25.35	12.68	49.57^{j}
100 Gy	10%	34.88	17.44	68.20^{e}	35.93	17.96	70.24^{d}	25.05	12.52	48.97^{i}	29.11	14.55	56.90^{g}
300 Gy		41.53	20.76	81.19^{a}	38.13	19.06	74.54^{c}	30.10	15.05	58.84^{f}	26.23	13.11	51.27^{i}
LSD (0.05)	**1.42104**												

Values followed by dissimilar letters with column are significantly different ($p < 0.05$); each value represents the mean of triplicates ± SD; *F.Y.*, fermentation yield.

exposure of cellulose accessibility making effective bioethanol conversion process (Fig. 5c, d). However, [49] noted that the best outcome obtained with diluted acid hydrolysis, which was then followed by solid-state fungal pretreatment and alkaline pretreatment.

In the present work, the yeast strain was irradiated with radioactive isotopes (cobalt-60) by 300 Gy. SEM photographs of native and mutant irradiated *S. cerevisiae* were illustrated in Fig. 6. Typical oval form of the native yeast appeared with smooth cell wall and small budding (Fig. 6a, b). Mutant yeast significantly decreased in size with deformed cell form and had some small wrinkles on the surface (Fig. 6c, d). The TEM of native and mutant strain for *S. cerevisiae* were represented in Fig. 7. Native cell had intact double layer of cell wall (CW), cell membrane, nucleus and organelles (Fig. 7a). Mutant strain had significant rupture of cell wall also disruption of vacuole (V) and changes in nucleus shape due to irradiation (Fig. 7b). Gamma irradiation is an electromagnetic radiation with high-energy, short wavelength, emitted by radioactive isotopes (cobalt-60 or cesium-137). Ionizing radiation shows some biological effects on cells because it can interact directly with essential vital cell components and indirectly through chemical compounds produced by radiolysis of certain molecules, especially water radicals [50, 51].

In addition, the potentiality of Inter simple sequence repeat analyses (ISSR) was utilized to evaluate the genetic variation of yeast (native and radiated) were represented in Table 3 and Fig. 8. Table 3 shows that a total of 136 bands were generated from yeast using 16 primers with an average polymorphism of 66.91%. In this study, each primer produced unique banding pattern of 3 (ISSR 5 and 16), 4 (ISSR 6, 8, and 12), 5 (ISSR 3, 4, and 9), 6 (ISSR 10, 13, and 15), 7 (ISSR 11, 18, and 20), 9 (ISSR 14), and 10 (ISSR 19) amplicons. ISSR 20 primer exhibited the highest discrimination between the native and radiated yeast, while ISSR 5, 6, 8, and 16 had 50% polymorphism (Table 3). Figure 8 illustrates the similarity between the two strains. It clarified that the radiated yeast was only 33% similar to the native one. So, all data revealed that the radiated yeast was highly divergent than the native one. Ionizing radiation can alter microorganisms chemically in a number of ways, in which DNA is the most critical target [50, 51].

Amounts of ethanol (g/L), fermentation yield, and % efficiency were evaluated in different strains of *S. cerevisiae* (native and mutant) after ethanol tolerance test for 12 h (Table 4). The yeast strain irradiated by 300 Gy and tolerated 10% ethanol for 12 h produced maximum amounts of ethanol (g/L), fermentation yield, and percentage efficiency recording 14.55 g/L, 29.11, and 56.90%, respectively. This was followed by strains irradiated with 100 Gy without and with 10% ethanol tolerance, which produced 13.85 and 13.74 g/L, 27.70 and 27.47, and 54.15 and 53.71% of

Table 7 Fermentation experiment of native and two irradiated best selected yeast strains inoculated in hydrolysate of pretreated *T. domingensis* with 4% sodium hypochlorite (the best hydrolyser)

Strains growth conditions		Ethanol amounts (g/l)	Fermentation yield	Efficiency (%)
Gamma irradiation (Gy)	Concentration of ethanol tolerance (%)			
Control-ve	–-	1.53	7.31	14.29[c]
100 Gy	–-	4.39	20.92	40.89[b]
300 Gy	10%	5.94	28.30	55.32[a]
LSD (0.5)		**1.2507**		

Values followed by dissimilar letters with column are significantly different ($p < 0.05$); each value represents the mean of triplicates ± SD.

Table 8 Fermentation experiment of the native and two irradiated best selected yeast strains applied on dried pretreated *T. domingensis* with 4% sodium hypochlorite and crude enzyme of *A. versicolor*

Strains growth conditions		Reducing Sugar	Ethanol amounts (g/l)	Fermentation yield	Efficiency (%)
Gamma irradiation (Gy)	Concentration of ethanol tolerance (%)				
control-ve	–-	19.00	3.06	24.30	40.10[b]
100 Gy	–-	18.40	3.21	26.57	42.83[c]
300 Gy	10%	19.20	5.94	28.30	55.32[a]
LSD (0.5)		**1.36156**			

Values followed by dissimilar letters with column are significantly different ($p < 0.05$); each value represents the mean of triplicates ± SD.

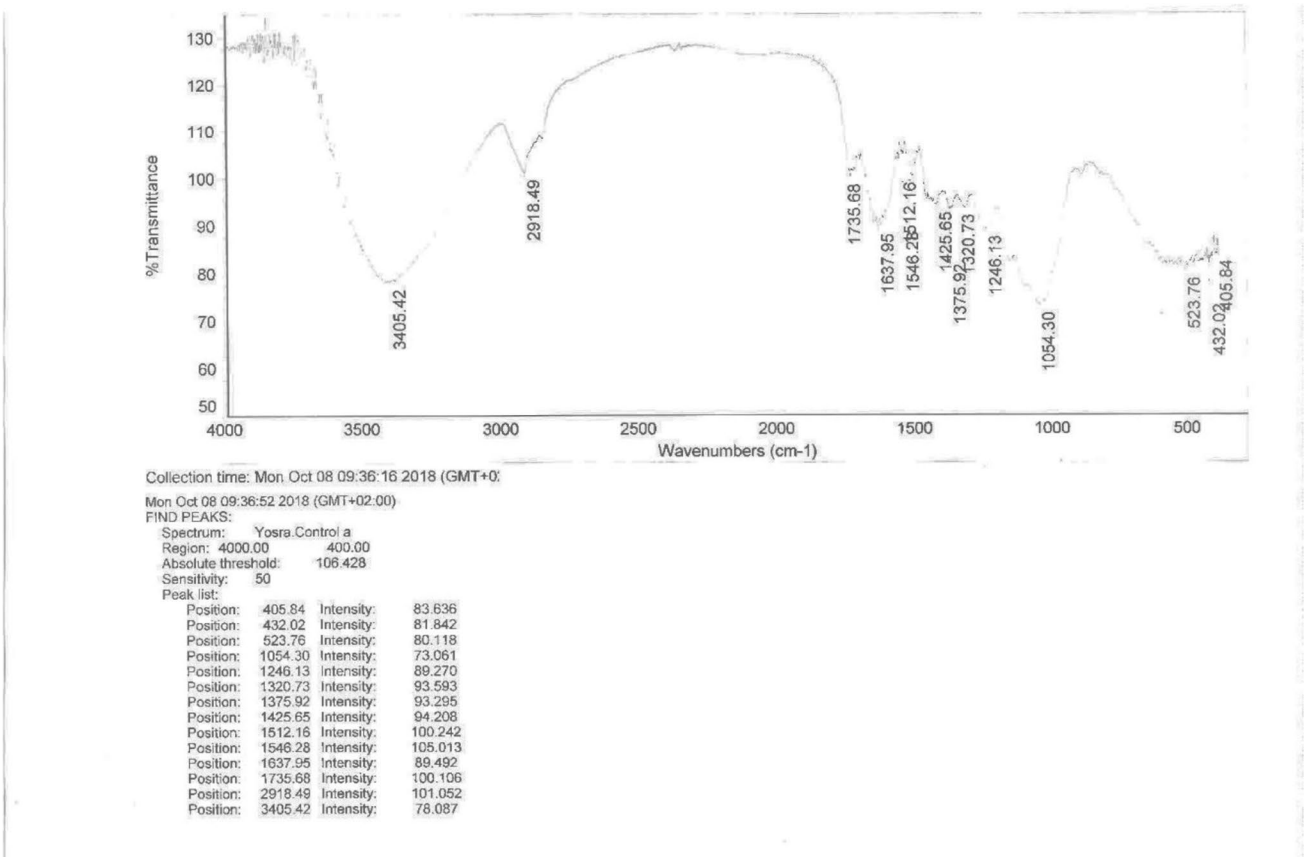

Fig. 9 The Fourier transform infrared spectroscopy (FTIR) of the native (untreated) *T. domingensis*

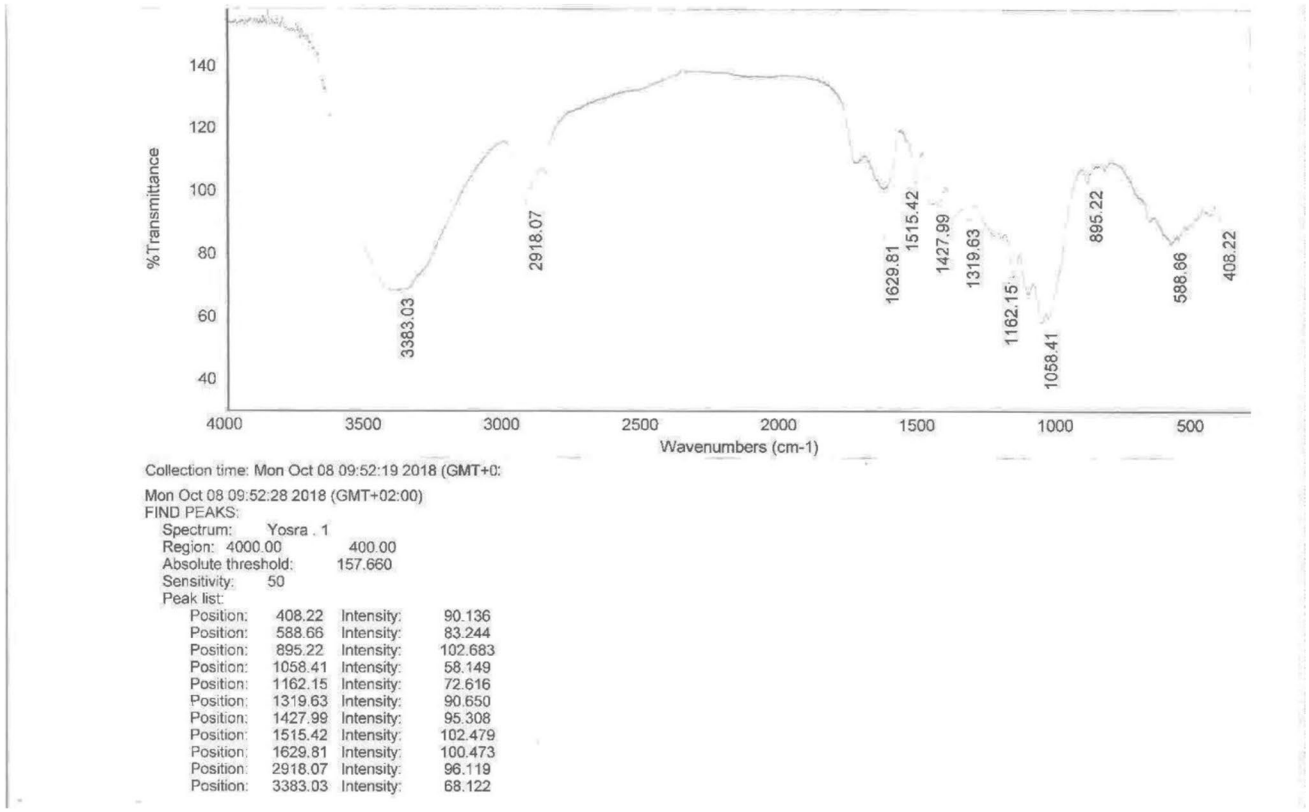

Fig. 10 The Fourier transform infrared spectroscopy (FTIR) of the treated *T. domingensis* using sulfuric acid

ethanol amounts (g/L), fermentation yield, and percentage efficiency, respectively.

Microorganisms like *S. cerevisiae* play a crucial role in the production of bioethanol by fermenting a wide variety of sugars to ethanol. Low doses of gamma irradiation have been shown to increase the activity of the enzyme alcohol-dehydrogenase in yeast strains [52–55]. Many investigators found that strains of *S. cerevisiae* exposed to lower doses of gamma irradiation (100–1000 Gy) increased their ability to grow and produce ethanol under stress [56–58].

Table 5 shows that after 24 h, the strains irradiated by 300 Gy and tolerated 10% ethanol still produce the maximum amounts of ethanol (g/L), fermentation yield, and percentage efficiency, which represented about 0.654-folds more than those recorded at 12 h. Next, strains irradiated with 100 Gy without ethanol tolerance also increased their high amount of ethanol (g/L), fermentation yield, and percentage efficiency by 0.738-folds.

Table 6 represents the fermentation of the three best selected strains and control (-ve) at different time intervals (12, 24, 36, and48 h). This experiment was used to select the best strain treatment and the time interval that produced the highest fermentation products. The fermentation activities of all strains increased reaching maximum at 24 h and then decline. Data also revealed that the strains irradiated by 300 Gy and tolerated 10% ethanol produced the highest amount of ethanol (g/L), fermentation yield, and percentage efficiency at 24 h. Strains irradiated with 100 Gy without ethanol tolerance expressed better fermentation activities than strains irradiated with 100 Gy with 10% ethanol tolerance along the experimental times.

Fermentation experiment of native and two irradiated best selected yeast strains inoculated on hydrolysate of pretreated *T. domingensis* with 4% Sodium Hypochlorite and crude enzyme of *A. versicolor*, was recorded in Table 7. The yeast strains irradiated by 300 Gy and tolerated 10% ethanol expressed the highest amounts of ethanol (5.94 g/L), fermentation yield (28.30) and % efficiency (55.32%).

Table 8 illustrates amounts of reducing sugars, ethanol (g/L), fermentation yield and % efficiency of the native and the best two irradiated strains after adding the crude enzyme of *A. versicolor* to the hydrolysate of pretreated *T. domingensis* with 4% sodium hypochlorite. Yeast strains irradiated by 300 Gy and tolerated 10% ethanol produced the highest amounts of reducing sugars (19.20), ethanol (5.94 g/L), fermentation yield (28.30), and percentage efficiency (55.32%).

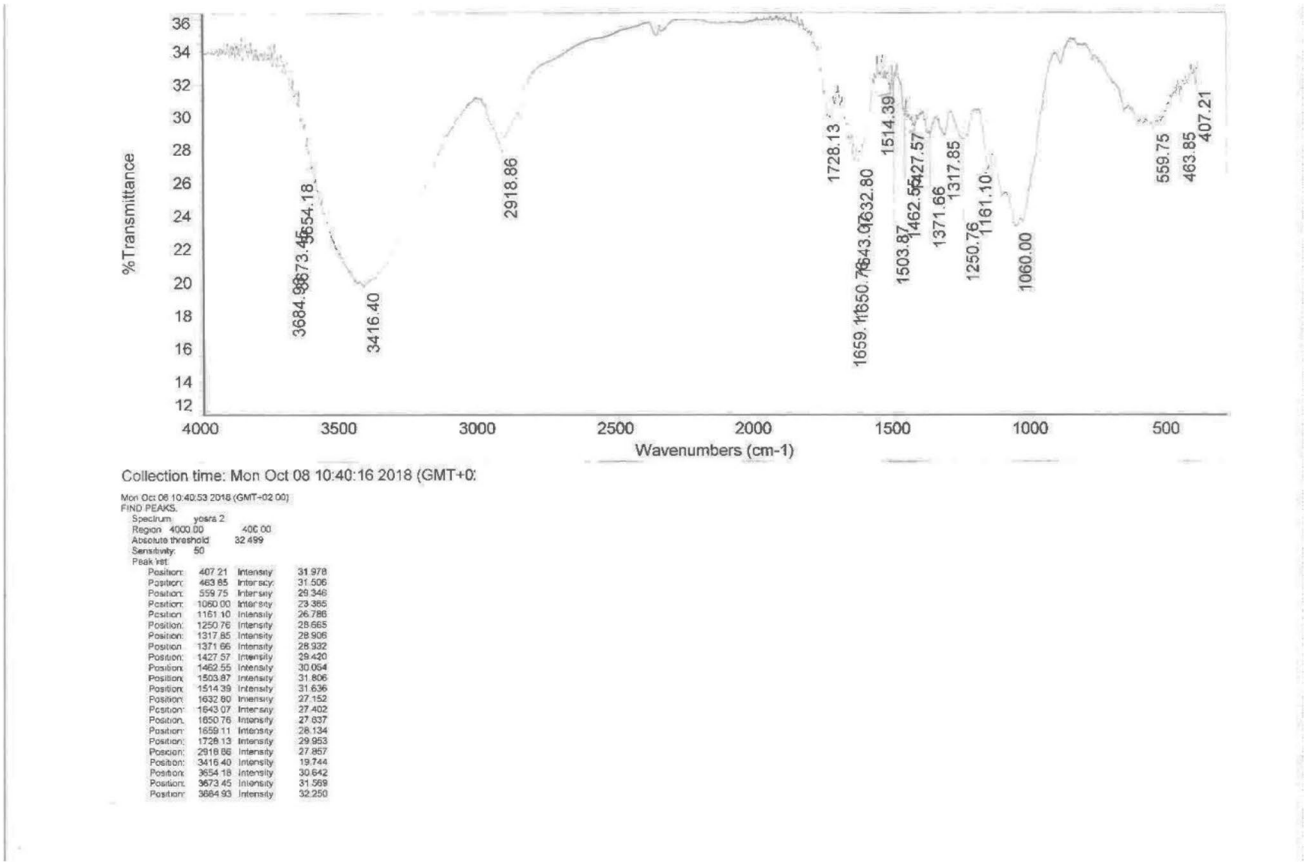

Fig. 11 The Fourier transform infrared spectroscopy (FTIR) of treated cattails using acetic acid

The Fourier transform infrared spectroscopy (FTIR) of treated and untreated *T. domingensis* fibers were illustrated in Figs. 9, 10, 11, 12, 13, 14, and 15.

Figure 9 shows the FTIR results of the native (untreated) *T. domingensis* leaf fibers, which displayed the vibration mode of fibrin and hydrocarbon in the fibers. The widest peak, 3405.42 cm^{-1}, could be linked to the stretching vibration of anti-free –OH, specifically that the waxiness of the fibers is high. The peak at 2918.49 cm^{-1} matches to the stretching vibration of -CH that is related to the presence of vegetable wax. There were three prominent peaks near 1637.95 cm^{-1}, 1512.16 cm^{-1}, and 1425.65 cm^{-1}, connected with the stretching vibration of C = O and C = C in lignin. The absorption band was caused by the stretching vibration of C = O, which existed in ketone, carboxyl, ester and xylan of 1735.68 cm^{-1} and 1246.13 cm^{-1}, 1375.92 cm^{-1} lignose. The peak at 1054.30 cm^{-1} of this affirmed the stretching vibration of C-O in cellulose, hemicelluloses, and lignose, which confirm the cellulosic type of the fiber.

Figure 10 illustrates the FTIR of the treated *T. domingensis* fibers using H_2SO_4. The figure showed the presence of widest peak (3383.03 cm^{-1}) linked to the stretching vibration of anti-free –OH or primary amine N–H. The peak at 2918.07 cm^{-1} still intact, and it matches to the stretching vibration of CH_2 that is related to the presence of vegetable wax. There was a peak near 1629.81 cm^{-1} that could be amide, 1515.42 cm^{-1} and 1427.99 cm^{-1}, connected with the stretching vibration of C = O and C = C in lignin. New band at 1162 cm^{-1} has appeared which reveal breakage of C = O into C-O of proteins and carbohydrates, stretching modes of the C–OH groups. Peak at 895.22 may represent vinylidene C-H out-of-plane bend. The peak at 1058.41 cm^{-1} affirmed the stretching vibration of C-O in cellulose, hemicelluloses, and lignose, indicating the presence of cellulose fiber.

The FTIR of treated Cattails using acetic acid (Fig. 11) revealed the presence of narrow peaks at 3684.93 cm^{-1}, 3673.45 cm^{-1}, and 3654.18 cm^{-1} could be linked to an oxygen related group, such as alcohol or phenol (illustrates the absence of hydrogen bonding). The peak at 3416.40 cm^{-1} may be due to OH stretch. The peak at 2918.86 cm^{-1} with low intensity match to the stretching vibration of CH_2 that is related to the presence of vegetable wax. A peak appeared at 1728.13 cm^{-1} may refer as ester or aldehyde. There were

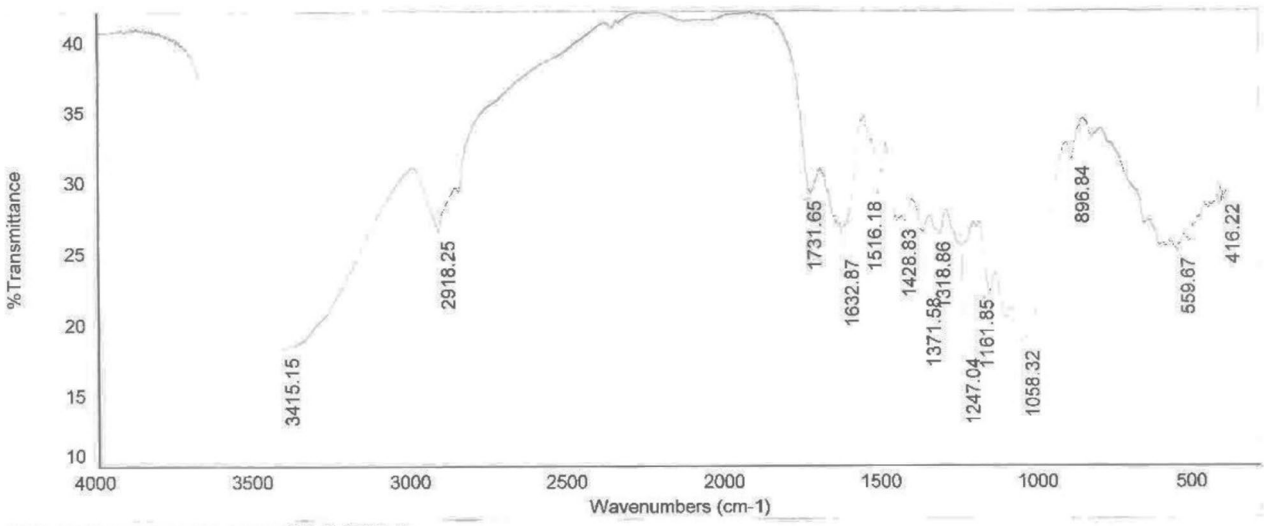

Collection time: Mon Oct 08 10:56:51 2018 (GMT+0:
Mon Oct 08 11:29:29 2018 (GMT+02:00)
FIND PEAKS:
Spectrum: Yosra , 3
Region: 4000.00 400.00
Absolute threshold: 41.568
Sensitivity: 50
Peak list:

Position:	416.22	Intensity:	28.333
Position:	559.67	Intensity:	25.138
Position:	896.84	Intensity:	31.610
Position:	1058.32	Intensity:	18.647
Position:	1161.85	Intensity:	22.166
Position:	1247.04	Intensity:	25.526
Position:	1318.86	Intensity:	26.302
Position:	1371.58	Intensity:	26.426
Position:	1428.83	Intensity:	27.150
Position:	1516.18	Intensity:	29.076
Position:	1632.87	Intensity:	26.543
Position:	1731.65	Intensity:	29.113
Position:	2918.25	Intensity:	26.482
Position:	3415.15	Intensity:	18.260

Fig. 12 The Fourier transform infrared spectroscopy (FTIR) of the treated *T. domingensis* fibers with hydrochloric acid

four successive peaks at 1659.11 cm^{-1}, 1650.76 cm^{-1}, 1643.07 cm^{-1}, and 1632.80 cm^{-1} that may be amide or ketones. The peak at 1060.0 cm^{-1} indicated the presence of phosphate ion, while peaks at 1514.39 cm^{-1} and 1427.57 cm^{-1} were related to the stretching vibration of C = O and C = C in lignin. However, peak at 1161.1 cm^{-1} has appeared which reveal very weak breakage of C = O into C-O of proteins and carbohydrates as its intensity is very low.

Figure 12 demonstrates the FTIR of the treated *T. domingensis* fibers with hydrochloric acid. It revealed that the presence of a widest peak, 3415.15 cm^{-1}, could be linked to the stretching vibration of anti-free –OH or aromatic primary amine NH stretch, specifically that the waxiness of the fibers is high. The peak at 2918.25 cm^{-1} matched to the stretching vibration of CH_2 that is related to the presence of vegetable wax. Three prominent peaks appeared near 1632.87 cm^{-1}, 1516.18 cm^{-1}, and 1428.83 cm^{-1}, still present and connected with the stretching vibration of C = O and C = C in lignin. The absorption band was caused by the stretching vibration of C = O, which existed in ketone, carboxyl, ester and xylan at 1731.65 cm^{-1} and 1247.04 cm^{-1}, 1371.58 cm^{-1} lignose. The appearance of a peak at 1161 cm^{-1} revealed the breakage of C = O into C-O of proteins and carbohydrates. New peak appeared at 896.84 cm^{-1} which may be due to C–O–C stretching or at β-glucosidic linkage in cellulose and hemicellulose.

The FTIR of the treated *T. domingensis* fibers with sodium hydroxide was illustrated in Fig. 13. A peak at 3852.66 cm^{-1} has newly appeared, and this corresponds to O–H stretching of primary and secondary hydroxyl group of cellulose, lignin, and hemicelluloses polymer. The widest peak, 3420.42 cm^{-1}, may be linked to the stretching vibration of hydroxyl group of hydrogen bond. The peak at 2917.96 cm^{-1} matched to the stretching vibration of CH_2 that is related to presence of vegetable wax. Three peaks appeared at 1634.92 cm^{-1}, 1558.15 cm^{-1}, and 1428.73 cm^{-1} and remain connected with the stretching vibration of C = O and C = C in lignin. The peak at 1373.24 cm^{-1} and

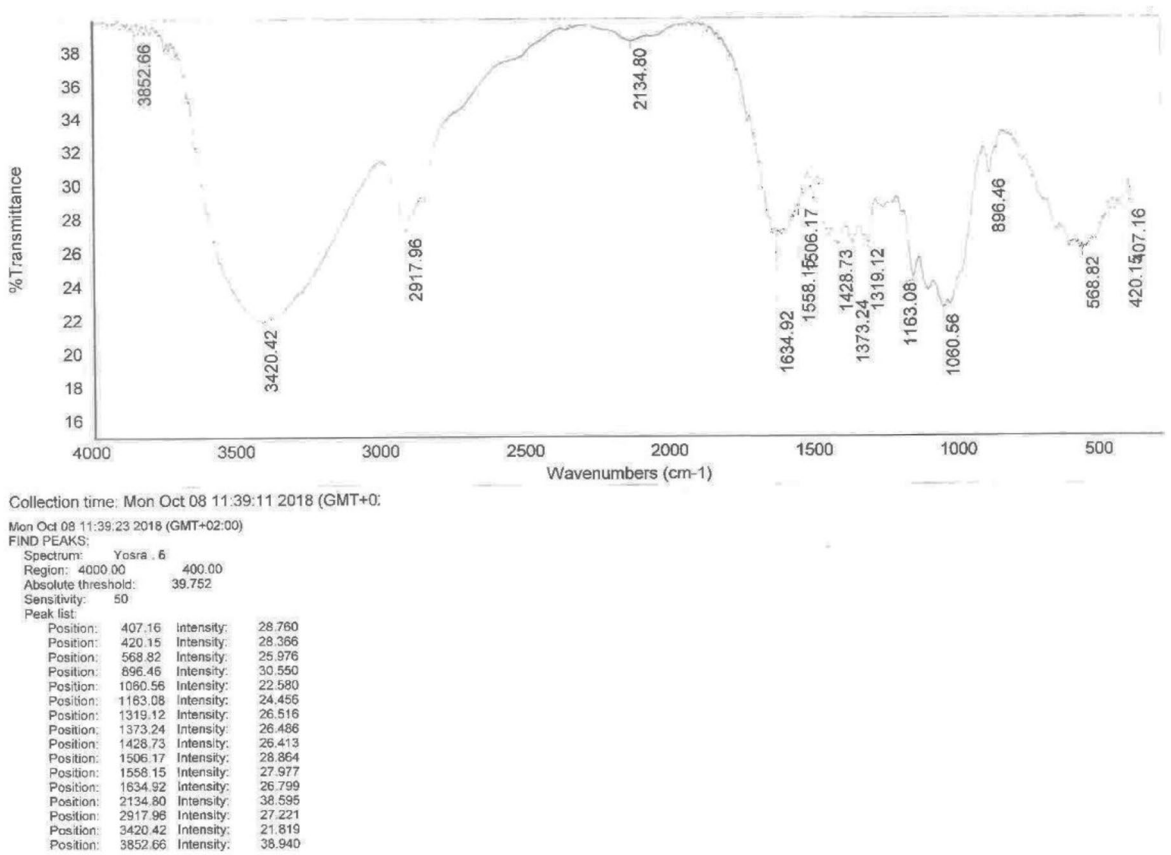

Fig. 13 The Fourier transform infrared spectroscopy (FTIR) of the treated *T. domingensis* fibers with sodium hydroxide

1319.12 cm^{-1} indicated the C-H banding, C-H stretching in CH3, and C-O stretching of C5 substituted aromatic units, respectively. The peak at 1163.08 cm^{-1} of this stretch has appeared which revealed the breakage of C = O into C-O of proteins and carbohydrates. Peaks appeared at 1060.58 cm^{-1} and 896.84 cm^{-1} which may be due to C-OH stretching vibration, C-O deformation, and C–O–C stretch or at β-glucosidic linkage in cellulose and hemicellulose, respectively.

Figure 14 displays the FTIR of the treated *T. domingensis* fibers with potassium hydroxide. A peak at 3850.53 cm^{-1} has newly appeared, and this corresponds to O–H stretching of primary and secondary hydroxyl group of cellulose, lignin, and hemicelluloses polymer. The widest peak, at 3417.59 cm^{-1}, was present. The peaks at 2918.30 cm^{-1} and 2850.49 cm^{-1} matched the stretching vibration of C-H that is related to presence of cellulose and hemicellulose. Two peaks at 1632.03 cm^{-1} and 1427.08 cm^{-1} still present and connected with the stretching vibration of C = O and C = C in lignin. The peak at 1317.96 cm^{-1} indicated C-H banding, C-H stretching in CH_3. The peak at 1162.60 cm^{-1} has appeared which reveal breakage of C = O into C-O of proteins and carbohydrates. Peaks presented at 1061.09 cm^{-1} and 897.06 cm^{-1} could be due to C-OH stretching vibration, C-O deformation, and C–O–C stretch or at β-glucosidic linkage in cellulose and hemicellulose, respectively. Three peaks presented at 580.85, 436.00, and 425.22 cm^{-1}, respectively, are may be attributed to Si–O-Si bending vibration.

Figure 15 exhibits the FTIR of the treated *T. domingensis* fibers with sodium hypochlorite. A peak at 3855.33 cm^{-1} has newly appeared and this corresponds to O–H stretching of primary and secondary hydroxyl group of cellulose, lignin, and hemicelluloses polymer. The widest peak at 3407.41 cm^{-1} was still present. The peak at 2917.57 cm^{-1} match to the stretching vibration of C-H that is related to the presence of cellulose and hemicellulose. Peak at 1735.25 cm^{-1} corresponds to C = O stretching of unconjugated ketone, carbonyls, and ester groups. Two peaks near 1637.69 cm^{-1} and 1425.97 cm^{-1} were also present. The peaks at 1375.36 cm^{-1} and 1322.08 cm^{-1} indicated C-H bending, C-H stretching in CH_3, and C-O stretching of C5-substituted aromatic units, respectively. The peak at

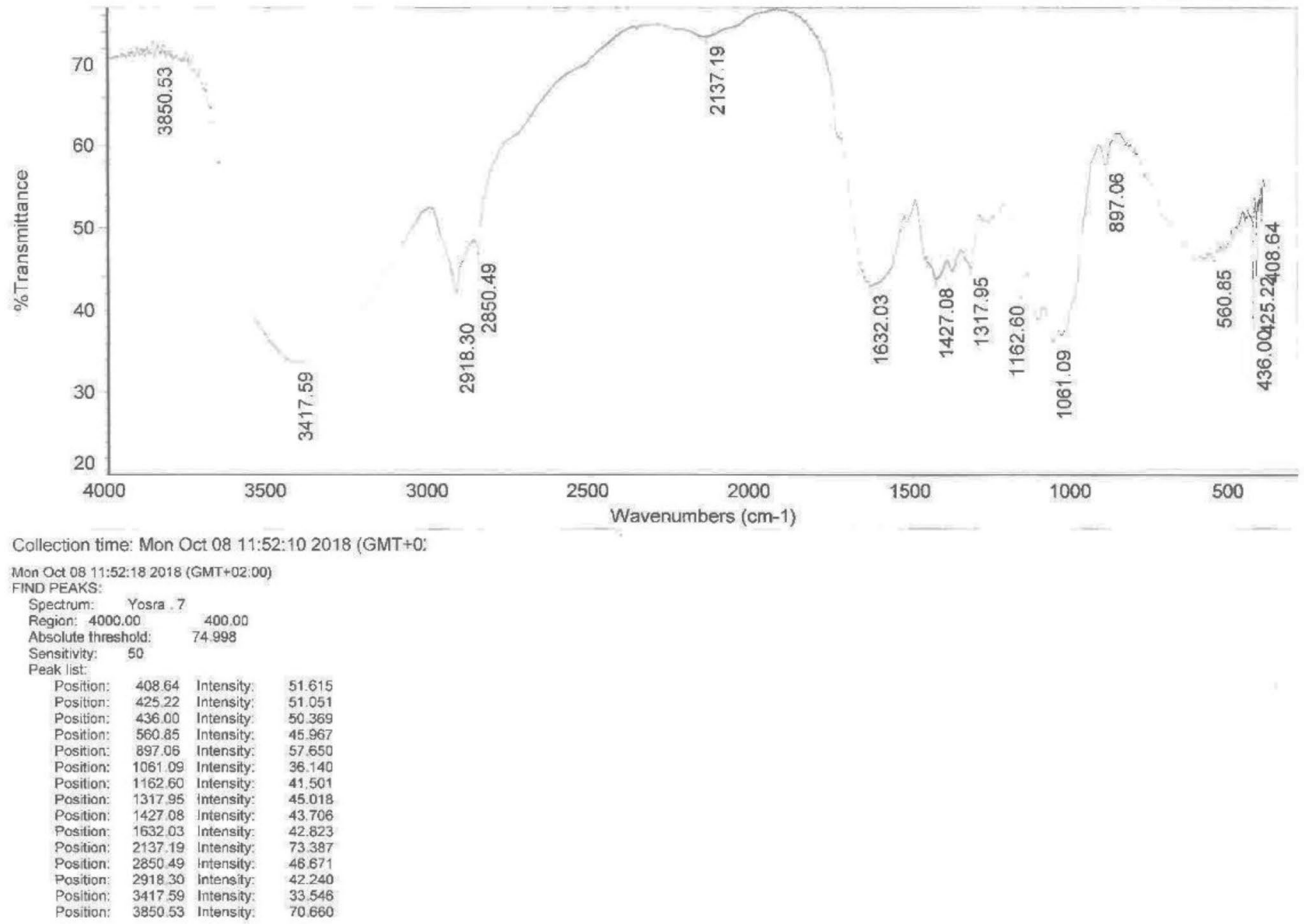

Fig. 14 The Fourier transform infrared spectroscopy (FTIR) of the treated *T. domingensis* fibers with potassium hydroxide

1058.84 cm^{-1} has appeared C-OH stretching vibration, C-O deformation. Peak has appeared at 900.29 cm^{-1} could be due to C–O–C stretch or at β-glucosidic linkage in cellulose and hemicellulose. Three peaks at 605.97, 438.04, and 424.28 cm^{-1}, respectively, were also present and may be attributed to C-(CH_2)n bending vibration.

By comparing the FTIR spectrum of the cattail leaves under different pretreatments, data recorded the presence of range of peaks from about 1000–4000 cm^{-1}. According to Du et al. (2019), the organic functional groups of polysaccharides in cattail, particularly O–H, N–H, and C = O, can be effectively identified by FTIR spectroscopy. Similar to our results, several investigators found that the FTIR spectrum obtained from cattail leaves and stem cell walls were very similar and revealed a collective range of bands from 400 to 4000 cm^{-1} [20, 59]. In details, the stretching vibration of the –OH groups cause of the signal at 3433.62 cm^{-1} and –CH stretching vibration of methyl or methylene groups in cellulose and hemicellulose was represented by a band at 2923.06 cm^{-1}. Also, signals at 1647.71 cm^{-1} and 1420.57 cm^{-1}, respectively, indicated the asymmetric and symmetric stretching of the carboxylate groups as mentioned by [60–62]. In addition, the angular vibration of the C–H bond of cellulose and hemicellulose was identified as the cause of band at about 1330.15–1375 cm^{-1} [59, 63]. The presence of peak at 1248.93 cm^{-1} reflect the asymmetric stretching vibration of the S = O bond [64]. The distinct peaks at ground 1000 to 1200 cm^{-1} revealed the presence of C–O–H side groups and C–O–C glycosidic band vibrations [59]. The C–O stretching vibration of the pyranose ring in the monosaccharide of cattail was identified as the source of the signal at 1043.03 cm^{-1} [65].

In addition, results revealed the presence of more functional groups below 1000 cm^{-1} in case of sodium hypochlorite and potassium hydroxide. These results confirmed the high amounts of reducing sugars after those pretreatments. The peak at about 895.99 cm^{-1} represents the β-glycosidic bands of the polysaccharide [66], while, band around

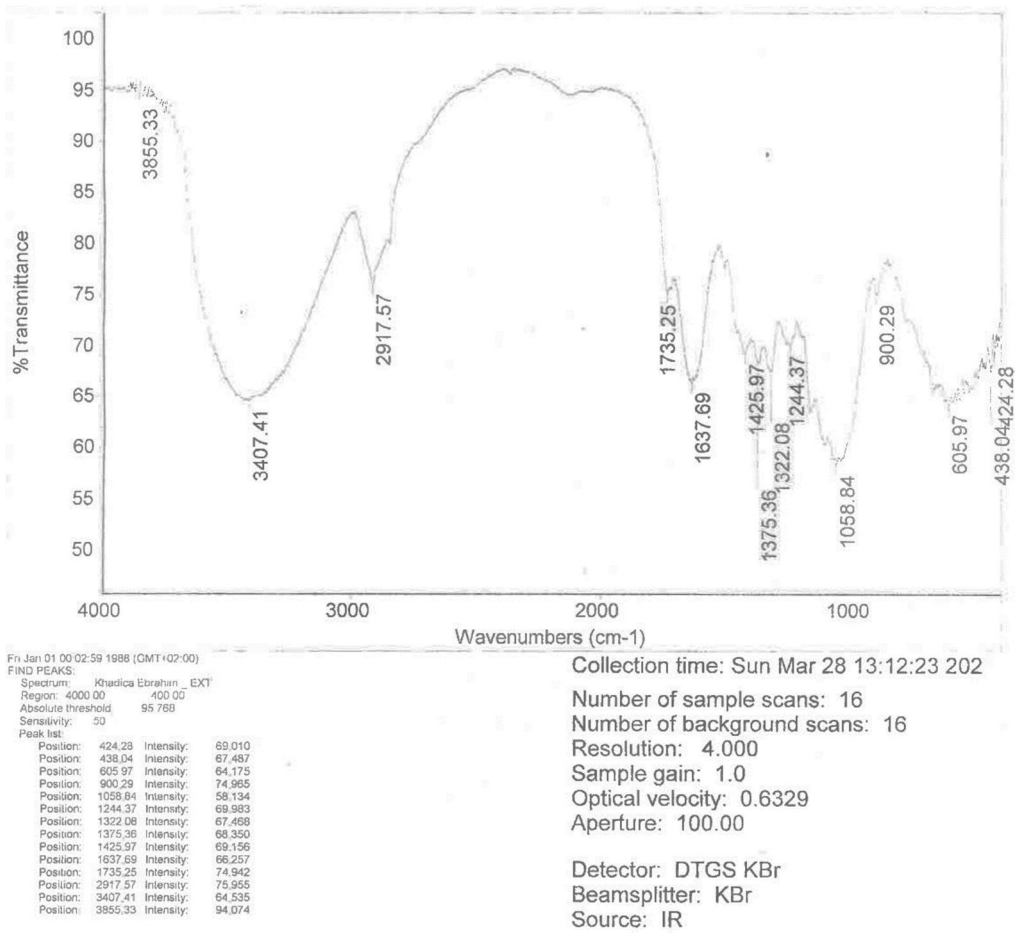

Fig. 15 The Fourier transform infrared spectroscopy (FTIR) of the treated *T. domingensis* fibers with sodium hypochlorite

528.52 cm^{-1} reflect the vibrations of C-(CH_2)n-($n \geq 4$) [67]. The stretch vibration of the carbohydrates' saccharide ring is responsible for the absorption band at 650–900 cm^{-1}, and the C–H out-of-plane bending vibration of the benzene ring of guaiacyl in the lignin is represented by the absorption peak inside this band at about 804 cm^{-1} [68–70].

The most effective method for determining a compound's structure and molecular chemistry is gas chromatography mass-spectrometry [71]. GC–MS device is a high selective, fast, and sensitive device used to characterize alcohol and impure components. It is a preferred method because it is quantitatively reproducible, provides a database, and is easy to analyze. Headspace gas chromatography with mass spectroscopy detection (HS-GC–MS method) has become a gold standard for ethanol and volatile compounds analysis in solid and liquid samples because it is mostly does not require any preliminary preparation, ease of automation, accuracy, sensitivity, and specificity [72, 73].

Figure 16a and b illustrate ethanol standard (50 µl/dL) that prepared in de-ionized water and replicated three times. One replicate of 50 µl/dL standard was analyzed in succession with a matrix matched internal standard (normal propanol at a concentration of 0.01% by volume (% v/v) in de-ionized water) blank prepared and analyzed after the 50 ul/dL standard.

Figure 16 showed sensitivity, thermostat stability, and carryover evaluation for instrumentation analyses, while analytical signal evaluation using IS peak areas improves precision and accuracy. These peaks were measured and calculated for ethanol and carried out considering peak ratios of the analyte to IS. The figure demonstrated excellent chromatographic selectivity, recorded retention times (Rt 2.224 to 2.324 min) of ethanol peaks (peak list: 30.1, 40.08, 41.07, and 42.1 m/z), and reviewed the chromatogram to confirm the absence of any contaminants [74].

Ethanol concentrations showed ability and evolution of the mutant *S. cerevisiae* during alcoholic fermentation that reflected the spread of *S. cerevisiae* uses in human manufacturing and led to the origin of numerous strains [75, 76]. Ethanol determination in each sample is quantified against

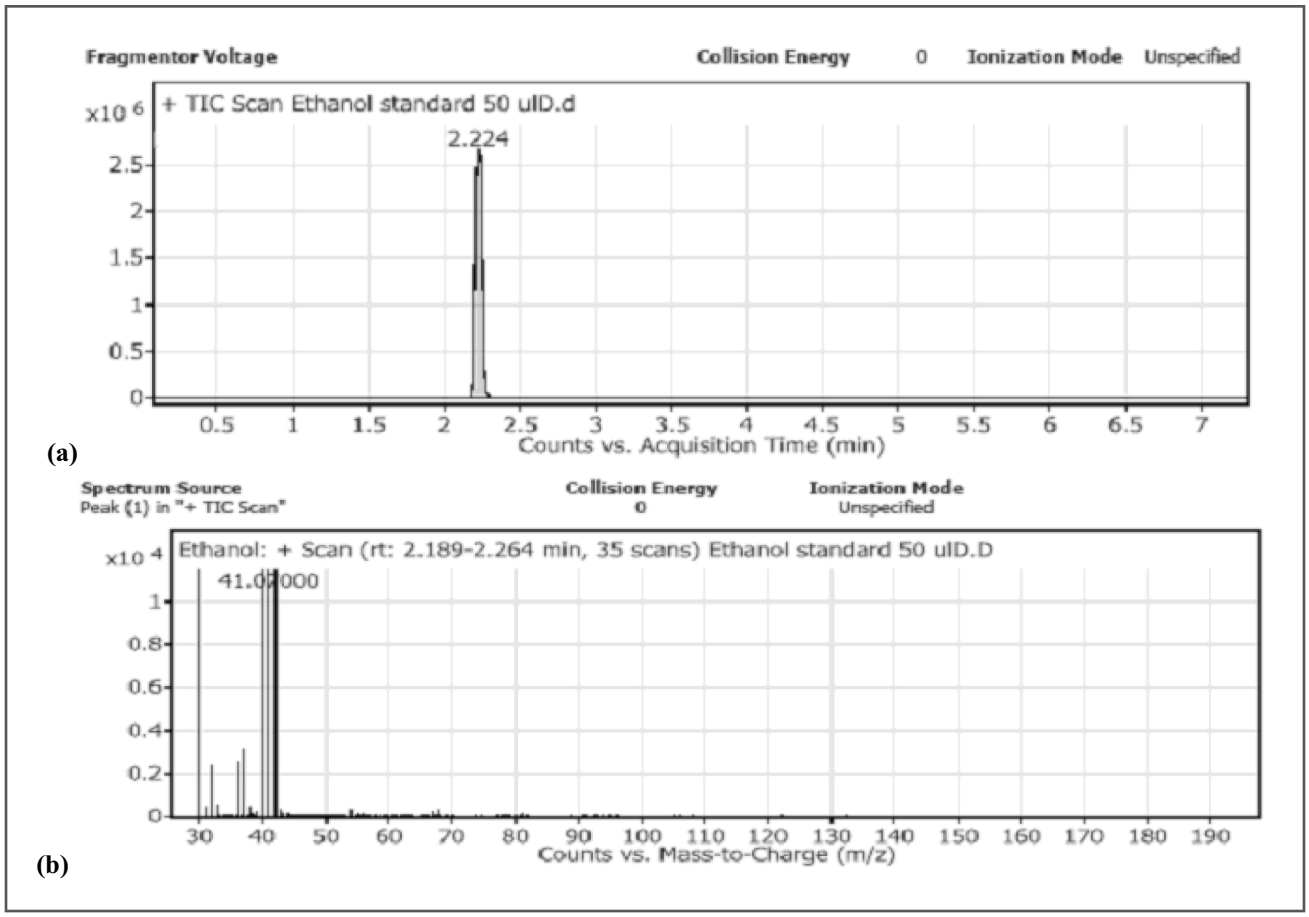

Fig. 16 Chromatogram of ethanol standard (50 µl) analysis using solvent residue HS-GC–MS

an external standard (ethanol standard 50 µl) and instrument calibration curve.

Figures 17, 18, and 19 show the availability of native and mutant *S. cerevisiae* yeast strains for reducing sugars consumption during alcoholic fermentation (AF) process. Figure 17a describes specific selectivity of ethanol using native *S. cerevisiae* strain that exhibits ethanol production capacity and is a representative host for bio-ethanol production [77, 78] at retention time (Rt 2.239–2.301 min) with area 3,479,702.01 and peak list: 30.1, 31.02, 41, 42.08, 43.07 m/z and four sugar products as shown in Fig. 17b at retention time (Rt 2.217–2.239 min).

The measurement of ethanol with native *S. cerevisiae* strain recorded 20.16 µl and many sugar compounds as by-products at the same retention time of ethanol under experimental condition during fermentation process [77, 78]. Figure 17c and d record determination of ethanol and five to six sugar products at Rt 2.253–2.277 min and Rt 7.929–8.130 min, respectively.

Figure 18a, b, and c record ethanol formation using mutant *S. cerevisiae* (100 Gy) during fermentation period (24 h). Figure 18a records specific selectivity of ethanol determination at their retention time (Rt 2.239 to 2.314 min) with fragmentation (peak list: 30.1, 40.08, 41.07, and 42.1 m/z), while Fig. 18b and c record ethanol formation and degradable sugars into alcohols and other end products peaks at Rt 2.239 to 2.314 min and Rt 12.007 to 12.401 min, respectively. The chromatograms showed mutant *S. cerevisiae* yeast (100 Gy) converts the sugars into ethanol under experimental conditions and by-products generated in the form of greenhouse gas CO_2 [79] and N-based compounds. The area of ethanol formation (4,733,004.67) recorded high yield of ethanol (about 27.42 µl) that confirmed with [45, 80].

Figure 19a and b record ethanol formation using radiated *S. cerevisiae* (300 Gy) during fermentation period (24 h). Figure 19a records specific selectivity of ethanol determination at their retention time (Rt 2.228 to 2.235 min) with fragmentation (peak list: 28.17, 29.16, 30.1, 40.07, 41.06 m/z). The chromatograms showed prevalent mutant *S. cerevisiae* (300 Gy) converts all sugars into ethanol under experimental conditions. During alcoholic

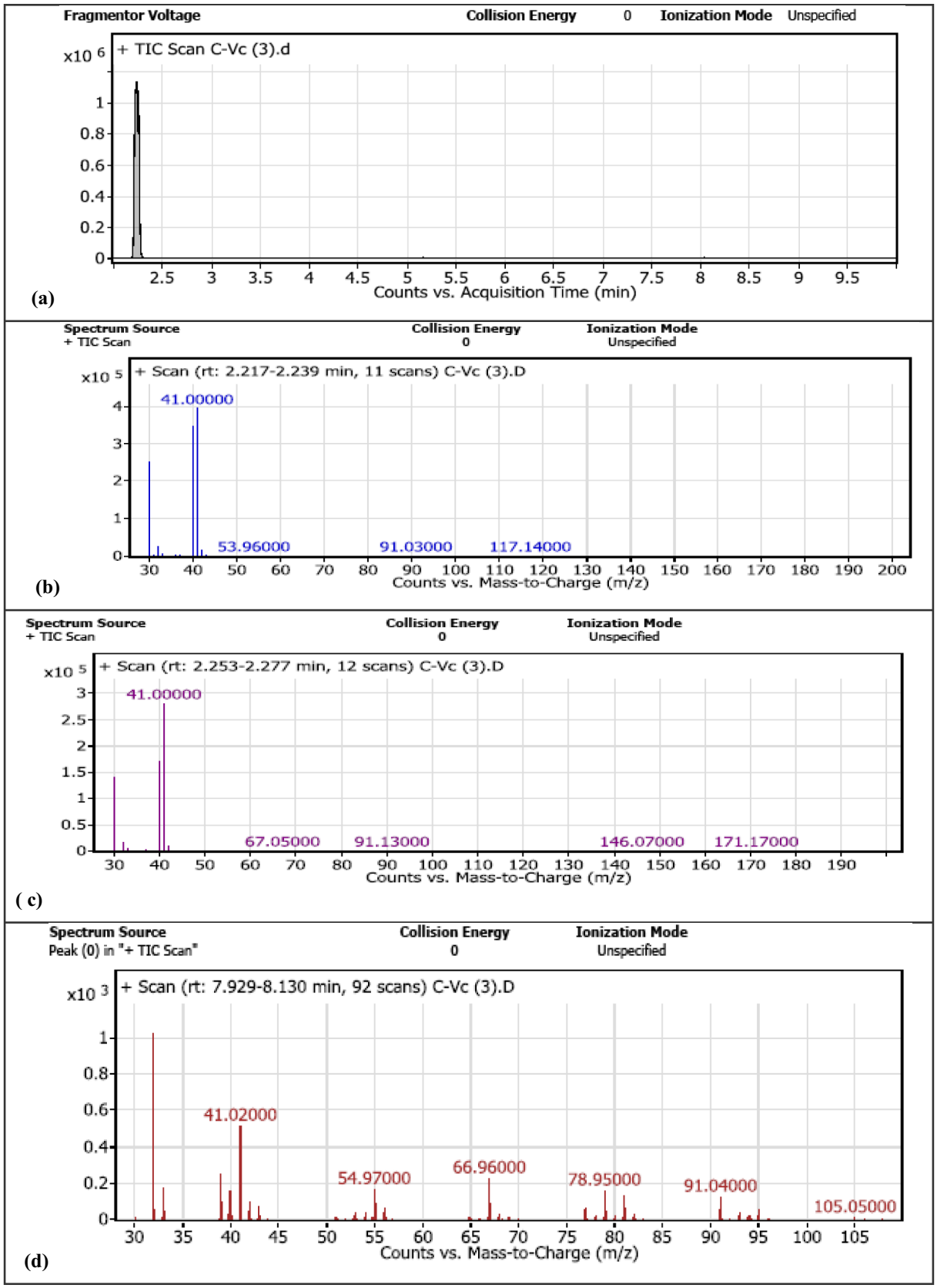

Fig. 17 Chromatogram of ethanol formation using native *S. cerevisiae*

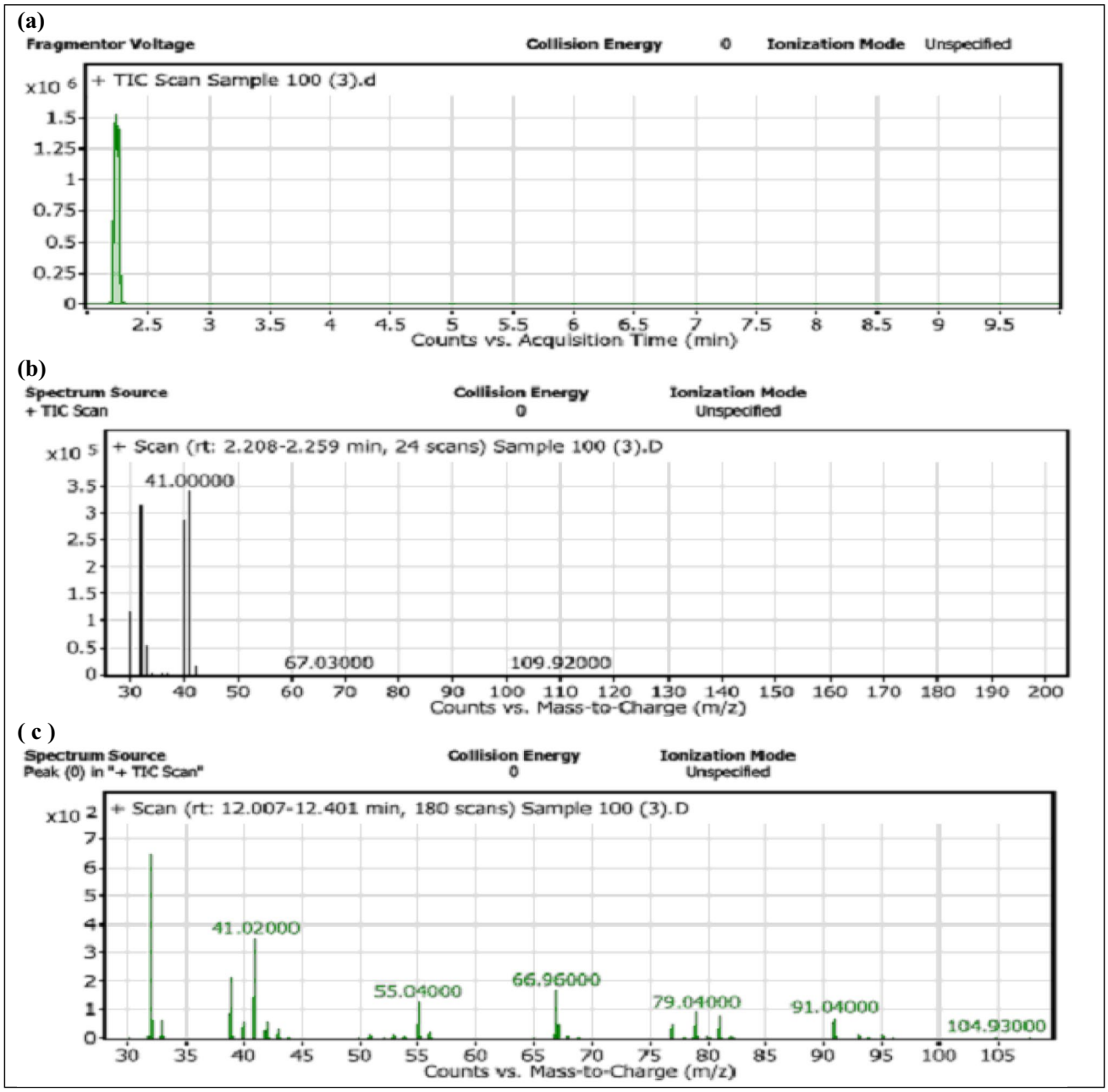

Fig. 18 Chromatogram of ethanol formation using radiated (100 Gy dose) *S. cerevisiae*

fermentation, *S. cerevisiae* produces ethanol with a yield close to all delegable sugars [79].

Mutant *S. cerevisiae* (300 Gy) indicated fast efficient glucose anaerobic metabolism, high ethanol productivity, and high yield which area of ethanol formation (97,710,120.18) recorded the highest yield of ethanol (about 566.09 µl). At industrial scale, ethanol is produced with a yield that is higher than 90% of the theoretical maximum [82] that confirmed with the obtained data industrial requirements production (0.51 g ethanol per g of consumed glucose) [82].

The obtained GC–MS revealed the presence of different compounds in biomass. These compounds represented

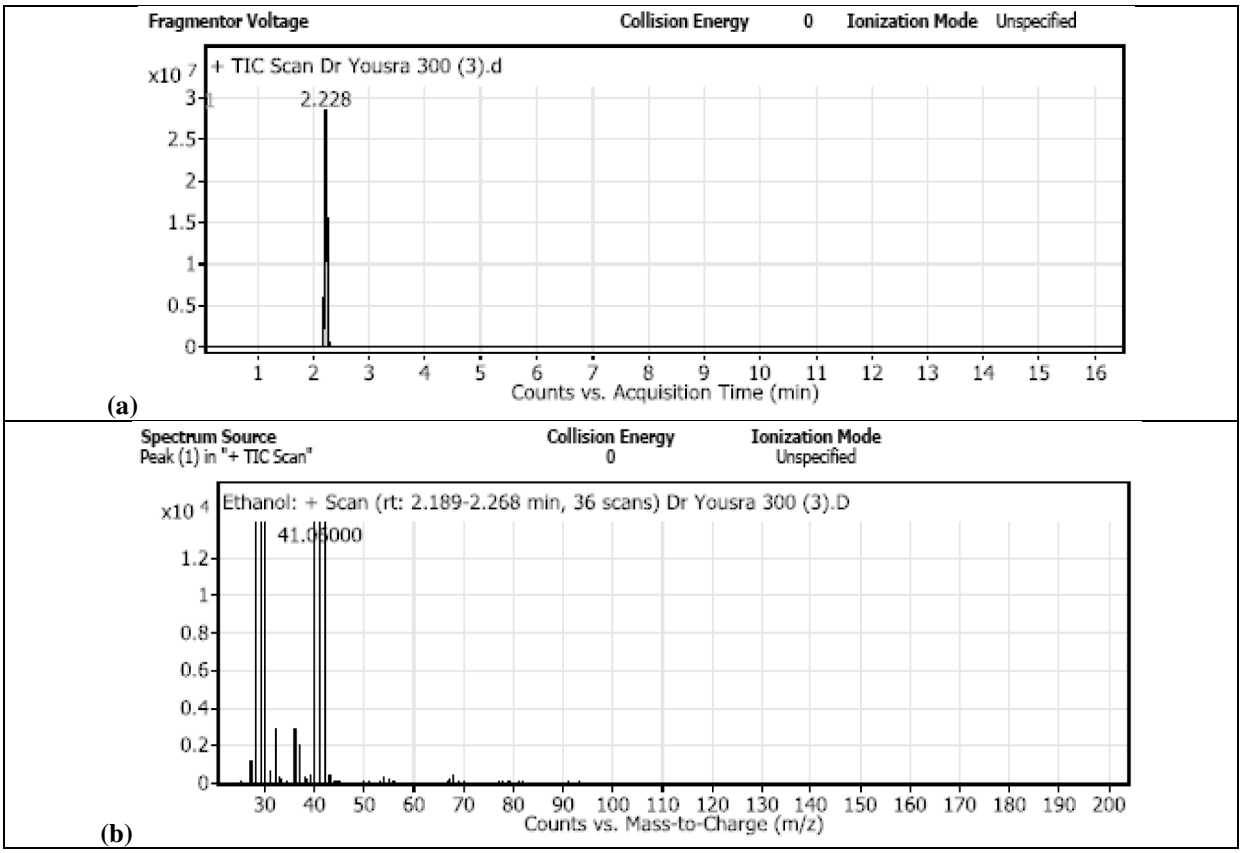

Fig. 19 Chromatogram of ethanol formation using radiated (300 Gy dose) *S. cerevisiae*

different classes including alkanes, alcohols, organic acid, ester, ketones, aldehydes, amides, and amines in which their functional groups were already confirmed by FTIR data.

Author contribution RMH, TMAA and YMMA Conceived and designed the experiments; RMH, TMAA,YMMA and KIME Performed the experiments; YMMA and MMY Collection of plant samples; RMH, TMAA,YMMA and KIME Analyzed the data; RMH, TMAA and YMMA Wrote the paper; RMH, TMAA and YMMA Revising of manuscript. All authors read and approved the final manuscript.

Funding Open access funding provided by The Science, Technology & Innovation Funding Authority (STDF) in cooperation with The Egyptian Knowledge Bank (EKB).

Data availability No data were taken from any database.

Declarations

Ethics approval and consent to participate Not applicable.

Competing interests The authors declare no competing interests.

References

1. Awasthi M, Kaur J, Rana S (2013) Bioethanol production through water hyacinth, *Eichhornia crassipes* via optimization of the pretreatment conditions. Intl J Emerg Technol Adv Eng 3(3):42–46
2. McKendry P (2002) Energy production from biomass (part 1): overview of biomass. Biores Technol 83(1):37–46
3. Elshahed M (2010) Microbiological aspects of biofuel production: current status and future directions. J Adv Res 1:103–111
4. Hoevers R (2011) Aquatic biofuels for local development. FACT Foundation, Amsterdam
5. Vega LP, Bautista KT, Campos H, Daza S, Vargas G (2024) Biofuel production in Latin America: a review for Argentina, Brazil, Mexico, Chile, Costa Rica and Colombia. Energy Rep 11:28–38
6. Galbe M, Zacchi G (2007) Pretreatment of lignocellulosic materials for efficient bioethanol production. In: Olsson, L. (eds)

Biofuels. Advances in Biochemical Engineering/Biotechnology, 108. Springer, Berlin, Heidelberg
7. Maripi et al. 2014. Production of bio-ethanol from aquatic weeds bio-ethanol. 4(1): 1–18.
8. Lewandowski I, Scurlock JMO, Lindvall E, Christou M (2003) The development and current status of perennial rhizomatous grasses as energy crops in the US and Europe. Biomass Bioenerg 25(4):335–361
9. Manivannan A, Narendhirakannan RT (2015) Bioethanol production from aquatic weed water hyacinth (Eichhornia crassipes) by yeast fermentation. Waste Biomass Valor 6(2):209–216
10. Apfelbaum SI (1985) Cattail (Typha spp.) management. Nat Areas J 5:9–17
11. Kucuk M, Demir H, Genel Y (2005) Supercritical fluid extraction of reed (Typha). Energy Sour 27:445–450
12. Zhang B, Shahbaz A, Wang L, Whitmore A, Riddick BA (2012) Fermentation of glucose and xylose in cattail processed by different pretreatment technologies. BioResources 7:2848–2859
13. Parisi F (1989) Advances in lignocellulosics hydrolysis and in the utilization of the hydrolysates. Adv Biochem Eng Biotechnol 38:53–87
14. Taherzadeh MJ (1999) Ethanol from lignocellulose: physiological effects of inhibitors and fermentation strategies, Chemical Reaction engineering. Chalmers University of Technmology, Goteborg, Sweden
15. Qureshi N, Manderson G (1995) Bioconversion of renewable resources into ethanol: an economic evaluation of selected hydrolysis, fermentation and membrane technologies. Energy Resources 17:241–265
16. Anasontzis GE, Christakopoulos P (2014) Challenges in ethanol production with Fusarium oxysporum through consolidated bioprocessing. Bioengin 5(6):1–3
17. Sridhar M, Sree NK, Rao LV (2002) Effect of UV radiation on thermotolerance, ethanol tolerance and osmotolerance of Saccharomyces cerevisiae VS1 and VS3 strains. Bioresour Technol 83:199–202
18. Eldin AM et al (2017) Synergetic saccharification by mixture of several fungal semi purified cellulose degrading enzymes. Middle East J Appl Sci 7(1):110–125
19. APHA (2017) Standard methods for the examination of water and wastewater, 23rd edn. American Public Health Association, Washington DC
20. Rebaque D, Martínez-Rubio R, Fornalé S, García-Angulo P, Alonso-Simón A, Álvarez JM, Caparros-Ruiz D, Acebes JL, Encina A (2017) Characterization of structural cell wall polysaccharides in cattail (*Typha latifolia*): evaluation as potential biofuel feedstock. Carbohyd Polym 175:679–688
21. Miller GL (1959) Use of dinitrosalicylic acid reagent for determination of reducing sugar. Anal Chem 31(3):426–428
22. Swelim MA, Dokhan AM, Abd-alsamee AM (2002) Biochemical studies on bioconversion of some lignocellulosic agricultural residues to economically valuable commodities biochemical studies on bioconversion of Amina Mahdy Mohammed
23. Kenealy WR, Dietrich DM (2004) Growth and fermentation responses of Phanerochaete chrysosporium to O2 limitation. Enz Microb Tech 34:490–498
24. Fatma H, El-Zaher A, Fadel M (2010) Production of bioethanol via enzymatic saccharification of rice straw by cellulase produced by Trichoderma reesei under solid state fermentation. N Y Sci J 3:72–78
25. Pilone GJ et al (1985) Determination of ethanol in wine by titrimetric and spectrophotometric dichromate methods: collaborative study. J Assoc Official Anal Chem 68(2):188–190
26. Bozzola JJ, Jones LDR (2002) Microscopy microanalysis. Microscopy Electron, Second Edition. 19–20
27. Popoola OO, Cooper JJ, Jakstys BP (1991) Application of ultramicrotomy to tem specimen preparation of particulate inclusion and composite materials. MRS Online Proc Libr 254:271–278
28. Reynolds ES et al (1963) The use of lead citrate at high pH as an electron-opaque stain in electron microscopy. J Cell Biol. 17(1):208–12
29. Shamseldean MM, Platzer EG (1989) Romanomermis culicivorax: penetration of larval mosquitoes. J Invert Pathol 54:191–199. (USA)
30. Abo-State MA, Mohamed SM, Shanab M, Ali HEA (2019) Effect of nutrients and gamma radiation on growth and lipid accumulation of chlorella vulgaris for biodiesel production. J Rad Res Appl Sci 12(1):332–342
31. Thammasittirong SN, Ranong TT, Thammasittirong A, Srisodsuk M (2013) Improvement of ethanol production by ethanoltolerant Saccharomyces Cerevisiae UVNR56. Springerplus 2(1):1–5
32. Stern RD (1991) CoStat-Statistical Software. California:CoHort Software (1989), pp. 302. Experimental Agric 27(1):87
33. Alexandropoulou M, Antonopoulou G, Fragkou E, Ntaikou I, Lyberatos G (2017) Fungal pretreatment of willow sawdust and its combination with alkaline treatment for enhancing biogas production. J Environ Manage 203:704–713
34. Arrisa S, Chayanoot S (2015) Optimization of enzymatic saccharification of alkali pretreated Typha angustifolia for glucose production. Intl J Chem Eng Appl 6:232–236
35. Zhang Bo et al (2010) Alkali pretreatment and enzymatic hydrolysis of cattails from constructed wetlands Bo Zhang, Abolghasem Shahbazi, Lijun Wang, Oumou Diallo and Allante Whitmore Department of Natural Resources and Environmental Design. Am J Eng Appl Sci 3(2):328–332
36. Zhang et al (2011) Dilute-sulfuric acid pretreatment of cattails for cellulose conversion. Biores Technol 102(19):9308–9312
37. Dashtban M, Schraft H, Qin W (2009) Fungal bioconversion of lignocellulosic residues; Opportunities & perspectives. Int J Biol Sci 5:578–595
38. Galanopoulou AP, Hatzinikolaou DG (2016) Fungi in consolidated bioprocessing of lignocellulosic materials. In: Fungal Applications in Sustainable Environmental Biotechnology, Springer, pp. 275–305
39. Wan C, Li Y (2012) Fungal pretreatment of lignocellulosic biomass. Biotechnol Adv 30(6):1447–1457
40. Wang FQ, Xie H, Chen W, Wang ET, Du FG, Song AD (2013) Biological pretreatment of corn stover with ligninolytic enzyme for high efficient enzymatic hydrolysis. Biores Technol 144:572–578
41. Castoldi R, Bracht A, de Morais GR, Baesso ML, Correa RCG, Peralta RA et al (2014) Biological pretreatment of Eucalyptus grandis sawdust with white- rot fungi: study of degradation patterns and saccharification kinetics. Chem Eng J 258:240–246
42. Sindhu R, Binod P, Pandey A (2016) Biological pretreatment of lignocellulosic biomass—an overview. Biores Technol 199:76–82
43. Mortazavi SM, Moghaddam MK (2010) An analysis of structure and properties of a natural cellulosic fiber (Leafiran). Fiber Polym 11:877
44. Jeya M, Zhang YW, Kim IW, Lee JK (2009) Enhanced saccharification of alkali-treated rice straw by cellulose from Trametes hirsuta and statistical optimization of hydrolysis conditions by RSM. Biores Technol 100:5155–5161
45. Kumar S, Singh SP, Mishra IM, Adhikari DK (2009) Recent advances in production of bioethanol from lignocellulosic biomass. Chem Eng Technol 2009 32:517–26
46. Taniguchi M, Takahashi D, Watanabe D, Sakai K, Hoshino K, Kouya T et al (2010) Effect of steam explosion pretreatment on treatment with Pleurotus ostreatus for the enzymatic hydrolysis of rice straw. J Biosci Bioeng 110:449–452

47. Satyanagalakshmi K et al (2011) Bioethanol production from acid pretreated water hyacinth by separate hydrolysis and fermentation. J Sci Ind Res 70(2):156–161
48. Sasmal S, Mohanty K (2018) Pretreatment of lignocellulosic biomass toward biofuel production. https://doi.org/10.1007/978-3-319-67678-4_9
49. Suhardi VSH, Prasai B, Samaha D, Boopathy R (2013) Evaluation of pretreatment methods for lignocellulosic ethanol production from energy cane variety L 79–1002. Int Biodeter Biodegr 85:683–687
50. Grecz N, Rowley DB, Matsuyama A (1983) The action of radiation on bacteria and viruses. In: "Preservation of food by ionizing radiation. Josephson Es; Peterson Ms (Ed). Vol. Ii. pp. 167–218. Boca Raton; Fl; Crc Press
51. Al-Sudany A, Wasan MZ, Al-Aubeidi HJA (2010) Detection of gamma radiation effect induced by Cobelt-60 on Escherichia coli cells. J Al-Nahrain Univ 13:129–133
52. Chakravarty B, Sen S (2001) Enhancement of regeneration potential and variability by γ-irradiation in cultured cells of Scilla indica. Biol Plant 44:189–193
53. Atia KS (2005) Co-immobilization of cyclo-hexanone mono-oxygenase and glucose-6- phosphate dehydrogenase onto polyethylenimine-porous agarose polymeric composite using γ-irradiation to use in biotechnological processes. Radiat Phys Chem 73:91–99
54. Akacha N, Zehlila A, Mejri S, Taieb J, Mohamed G (2008) Effect of gamma ray on activity and stability of alcohol dehydrogenase from Saccharomyces cerevisiae. Biochem Eng J 40:184–188
55. Abdel-Fattah WR, Fadil M, Nigam P, Banat IM (2000) Isolation of thermotolerant ethanologenic yeasts and use of selected strains in industrial scale fermentation in an Egyptian distillery. Biotechnol Bioeng 68:531–535
56. Abosereh NA, Soliman EAM, Abd El-Khalek BA (2006) Mutation induction for genetic improvement of Saccharomyces boulardii which used as probiotic yeast Res. J Agr Biol Sci 2(6):478–482
57. Edgardo A, Carolina P, Manuel R, Juanita F, Jaime B (2008). Selection of thermotolerant yeast strains S. cerevisiae for bioethanol production. Enzyme Microb Tech 2:007
58. Zheng T, Gu D, Wang X, Shen X, Yan L, Zhang W, Pu Y, Ge C, Fan J (2020) Purification, characterization and immunomodulatory activity of polysaccharides from Leccinum crocipodium (Letellier.) Watliag, Int J Biol Macromol. 148:647–656
59. Kathirselvam M, Kumaravel A, Arthanarieswaran VP, Saravanakumar SS (2019) Isolation and characterization of cellulose fibers from Thespesia populnea barks: a study on physicochemical and structural properties. Int J Biol Macromol 129:396–406
60. Prado KS, Spinace MAS (2019) Isolation and characterization of cellulose nanocrystals from pineapple crown waste and their potential uses. Int J Biol Macromol 122:410–416
61. Košťálová Z, Hromádková Z (2019) Structural characterisation of polysaccharides from roasted hazelnut skins. Food Chem 286:179–184
62. El Oudiani A, Msahli S, Sakli F (2017) In-depth study of agave fiber structure using Fourier transform infrared spectroscopy. Carbohydr Polym 164:242–248
63. Yuan F, Gao Z, Liu W, Li H, Zhang Y, Feng Y, Song X, Wang W, Zhang J, Huang C, Jia L, Characterization, antioxidant. (2019) Antiaging and organ protective effects of sulfated polysaccharides from Flammulina velutipes. Molecules 24 3517
64. Ma JS, Liu H, Han CR, Zeng SJ, Xu XJ, Lu DJ, He HJ (2020) Extraction, characterization and antioxidant activity of polysaccharide from Pouteria campechiana seed. Carbohyd Polym 142:232–236
65. Wang Y, Guo M (2020) Purification and structural characterization of polysaccharides isolated from Auricularia cornea var. Li, Carbohyd Poly 230:115680.
66. Yi Y, Huang XY, Zhong ZT, Huang F, Li SY, Wang LM, Min T, Wang HX (2019) Structural and biological properties of polysaccharides from lotus root. Int J Biol Macromol 130:454–461
67. De Rosa IM, Kenny JM, Maniruzzaman M, Moniruzzaman M, Monti M, Puglia D, Santulli C, Sarasini F (2011) Effect of chemical treatments on the mechanical and thermal behaviour of okra (Abelmoschus esculentus) fibres. Compos Sci Technol 71(2):246–254
68. Cheng D, Weng B, Chen Y, Zhai S, Wang C, Xu R, Guo J, Lv Y, Shi L, Guo Y (2020) Characterization of potential cellulose fiber from luffa vine: a study on physicochemical and structural properties. Int J Biol Macromol. 164:2247–2257.
69. Wu S et al. (2021) Characterization of potential cellulose fiber from cattail fiber : a study on micro / nano structure and other properties. Intl J Biol Macromol 193(PA): 27–37.
70. Yasmin T, Asghar A, Ahmad MS et al (2023) Biorefinery potential of Typha domingensis biomass to produce bioenergy and biochemicals assessed through pyrolysis, thermogravimetry, and TG-FTIR-GCMS-based study. Biomass Conv Bioref 13:10957–10969
71. Bedner M, Murray J, Urbas AA, MacCrehan WA, Wilson WB (2021) Comparison of measurement methods for alcohol-based hand sanitizers, NIST Interagency/Internal Report (NISTIR), National Institute of Standards and Technology. Gaithersburg 2021
72. Varlik S, Bayrak G, Demircelik IP, Isbir Turan AA (2022) Gas chromatography-mass spectroscopy analysis and antibacterial tests of commercial hand sanitizers. Hittite J Sci Eng 9(1):37–44
73. Sy H, Chan M, Finley J (2023) Determination of ethanol content in water kefir using headspace gas chromatography with mass spectrometry detection: matrix extension and methanol characterization. J AOAC Intl 106 (2):348–355
74. Legras J-L, Galeote V, Bigey F, Camarasa C, Marsit S, Nidelet T, Sanchez I, Couloux A, Guy J, Franco-Duarte R, Marcet-Houben M, Gabaldon T, Schuller D, Sampaio J P, Dequin S (2018) Adaptation of S. cerevisiae to fermented food environments reveals remarkable genome plasticity and the footprints of domestication. Mol Biol Evol 35 (7):1712–1727
75. Laura P, Elisa G, Antonella C, Enrico TV, Christos T, Garcia-Moruno E (2021) Grapes and Wine book - Chapter 8: an overview on saccharomyces cerevisiae indigenous strains selection methods. Edited by Antonio Morata and Iris Loira and Carmen González, IntechOpen, 2021
76. Favaro L, Jansen T, van Zyl WH (2019) Exploring industrial and natural Saccharomyces cerevisiae strains for the bio-based economy from biomass: the case of bioethanol. Critical Rev Biotechnol39 (6):800–816
77. Ruchala J, Kurylenko OO, Dmytruk KV, Sibirny AA (2019) Construction of advanced producers of first and second-generation ethanol in Saccharomyces cerevisiae and selected species of non-conventional yeasts (Scheffersomyces stipitis, Ogataea polymorpha). J Industr Microbiol Biotechnol 47:109–32
78. Yatabe F, Seike T, Okahashi N, Ishii J, Matsuda F (2023) Improvement of ethanol and 2,3-butanediol production in Saccharomyces cerevisiae by ATP wasting. Microbial Cell Factories, 22, ID: 204, 2023
79. Achinas S, Euverink GJW (2016) Consolidated briefing of biochemical ethanol production from lignocellulosic biomass. Electron J Biotechnol 23:44–53
80. Justyna R, Olena OK, Kostyantyn VD, Andriy AS, (2021) Construction of advanced producers of first- and second-generation ethanol in *Saccharomyces cerevisiae* and selected species of non-conventional yeasts (*Scheffersomyces stipitis, Ogataea polymorpha*). J Industr Microbiol Biotechnol 2020; 47(1):109–132
81. Walaa E, Sanaa S, Emad S, Rehab H (2021) Plant growth regulators from microalgae biomass and their impact on the genetic fidelity of canola and tomato plantlets. Biomass Convers Biorefin 13:3. https://doi.org/10.1007/s13399-021-02097-2